JGR Atmospheres

RESEARCH ARTICLE
10.1029/2023JD040507

Key Points:

- Ammonium nitrate formation in summertime over northeastern Colorado is ammonia-rich and nitrate-limited
- Observations and model analyses indicate that <300 m agl, ammonium nitrate is usually <1 μg m^{-3} and inhibited by warmer temperatures
- Cooler temperatures during spring/autumn and winter in northeastern Colorado are predicted to support substantial NH_4NO_3 formation

Supporting Information:

Supporting Information may be found in the online version of this article.

Correspondence to:

J. R. Pierce and E. Li,
jeffrey.pierce@colostate.edu;
en.li@colostate.edu

Citation:

Li, E., Pierce, J. R., Juncosa Calahorrano, J. F., Sullivan, A. P., Pollack, I. B., Roscioli, J. R., et al. (2024). Inorganic nitrogen gas-aerosol partitioning in and around animal feeding operations in northeastern Colorado in late summer 2021. *Journal of Geophysical Research: Atmospheres*, *129*, e2023JD040507. https://doi.org/10.1029/2023JD040507

Received 3 DEC 2023
Accepted 18 MAY 2024

Inorganic Nitrogen Gas-Aerosol Partitioning in and Around Animal Feeding Operations in Northeastern Colorado in Late Summer 2021

En Li[1], Jeffrey R. Pierce[1], Julieta F. Juncosa Calahorrano[1], Amy P. Sullivan[1], Ilana B. Pollack[1], Joseph R. Roscioli[2], Dana R. Caulton[3], Megan E. McCabe[3], Shantanu H. Jathar[4], and Emily V. Fischer[1]

[1]Department of Atmospheric Science, Colorado State University, Fort Collins, CO, USA, [2]Aerodyne Research Inc., Billerica, MA, USA, [3]Department of Atmospheric Science, University of Wyoming, Laramie, WY, USA, [4]Department of Mechanical Engineering, Colorado State University, Fort Collins, CO, USA

Abstract Ammonia (NH_3) from animal feeding operations (AFOs) is an important source of reactive nitrogen in the US, but despite its ramifications for air quality and ecosystem health, its near-source evolution remains understudied. To this end, Phase I of the Transport and Transformation of Ammonia (TRANS^{2}Am) field campaign was conducted in the northeastern Colorado Front Range in summer 2021 and characterized atmospheric composition downwind of AFOs during 10 research flights. Airborne measurements of NH_3, nitric acid (HNO_3), and a suite of water-soluble aerosol species collected onboard the University of Wyoming King Air research aircraft present an opportunity to investigate the sensitivity of particulate matter (PM) formation to AFO emissions. We couple the observations with thermodynamic modeling to predict the seasonality of ammonium nitrate (NH_4NO_3) formation. We find that during TRANS^{2}Am northeastern Colorado is consistently in the NH_3-rich and HNO_3-limited NH_4NO_3 formation regime. Further investigation using the Extended Aerosol Inorganics Model reveals that summertime temperatures (mean: 23°C) of northeastern Colorado, especially near the surface, inhibit NH_4NO_3 formation despite high NH_3 concentrations (max: $\leq$114 ppbv). Finally, we model spring/autumn and winter conditions to explore the seasonality of NH_4NO_3 formation and find that cooler temperatures could support substantially more NH_4NO_3 formation. Whereas NH_4NO_3 only exceeds 1 μg m^{-3} ~10% of the time in summer, modeled NH_4NO_3 would exceed 1 μg m^{-3} 61% (88%) of the time in spring/autumn (winter), with a 10°C (20°C) temperature decrease relative to the campaign.

Plain Language Summary Animal feeding operations (AFO; i.e., feedlots for large-scale meat/dairy production) emit large amounts of ammonia into the atmosphere. Gas-phase ammonia can change into aerosol-phase ammonium (i.e., gas-aerosol partitioning) and contribute to particulate matter air pollution. In this study, we try to understand whether ammonia emitted from AFOs is forming aerosols, and if so, what mechanisms are governing the gas-aerosol transfer between ammonia and ammonium. To do so, we flew a research aircraft downwind of several AFOs in northeastern Colorado in summer 2021 and measured a suite of gases and aerosols (and temperature and relative humidity). We measured high amounts of ammonia gas and low amounts of ammonium aerosols, so the observations alone only indicate that ammonia from AFOs likely is not a significant source of summertime $PM_{2.5}$. We then put our observations into an aerosol thermodynamic model and learned that summertime northeastern Colorado is too hot and dry to favor aerosol formation despite high amounts of ammonia. We also make some approximations of spring/autumn and winter conditions in the model and learn that the cooler temperatures could potentially support substantial $PM_{2.5}$ formation. This means that ammonia from AFOs could be a significant source of wintertime $PM_{2.5}$ pollution in Northeastern Colorado.

1. Introduction

Ammonia (NH_3) from agricultural activity accounts for over 80% of global emissions, with 50% from livestock manure and 30% from crop fertilizer (Wyer et al., 2022). Global NH_3 emissions and agricultural output have increased dramatically since the invention of the Haber-Bosch process in the early 20th century (Erisman et al., 2008; Galloway et al., 2004) and are projected to continue to increase in the near future to meet food security demands from a growing global population (Galloway et al., 2004; van Vuuren et al., 2011). The United States (US) is the third largest contributor of global NH_3 emissions (Liu et al., 2022). In the US, where NH_3 emissions remain unregulated, agriculture accounts for over 80% of domestic NH_3 emissions, with almost 50% of total domestic emissions attributable to livestock production (NEI, 2020).

Animal feeding operations (AFOs) are major agricultural point sources of NH_3. AFOs emit NH_3 when nitrogen-containing compounds (e.g., urea and undigested proteins) in livestock waste decompose and volatilize (Behera et al., 2013; Wyer et al., 2022). The volatilization of NH_3 from AFOs is affected by waste management/storage practices and ambient conditions such as temperature, soil water content, wind speed, etc. (Behera et al., 2013; Hristov et al., 2011), with temperature being the most significant meteorological parameter (Robarge et al., 2002). Thus, in regions with intensive animal agriculture such as Northern Colorado, NH_3 concentrations peak in the summer when AFO emissions are generally highest (e.g., Benedict, Day, et al., 2013; Eilerman et al., 2016; Wang et al., 2020). In Northern Colorado, NH_3 exhibits strong spatial gradients (e.g., Benedict, Day, et al., 2013) due to its short lifetime (hours-weeks) (Evangeliou et al., 2021; Juncosa Calahorrano et al., 2023; Luo et al., 2022), and NH_3 hotspots can be large enough to identify and trace back to individual AFOs via satellite imagery (Van Damme et al., 2018). Under upslope wind conditions, AFOs in Northern Colorado have also been shown to contribute significantly to nitrogen deposition and affect ecosystem health in Rocky Mountain National Park (e.g., Benedict et al., 2018; Pan et al., 2021).

Ammonia is the most abundant alkaline gas in the atmosphere and important for fine particulate matter ($PM_{2.5}$) formation. Under thermodynamically favorable conditions, gaseous NH_3 can partition to form aerosol-phase ammonium (NH_4^+), which can degrade ecosystem health via soil acidification (Tian & Niu, 2015) and eutrophication (Zhan et al., 2017). In the particle phase, NH_4^+ can also contribute to a significant fraction of inorganic $PM_{2.5}$ mass (Jimenez et al., 2009), which has adverse effects on human health (Pope et al., 2009) and visibility (Hand et al., 2020).

The inorganic gas-aerosol partitioning of NH_3-NH_4^+ is determined by complex, non-linear relationships between meteorological conditions and atmospheric composition. In the atmosphere, sulfuric acid (H_2SO_4) readily condenses into an acidic aerosol (Ayers et al., 1980; Kulmala & Laaksonen, 1990; Roedel, 1979), and any NH_3 present will partition to the aerosol phase to form $(NH_4)_2SO_4$ until sulfate (SO_4^{2-}) is fully neutralized (Bassett & Seinfeld, 1983). Next, any remaining NH_3 can react with HNO_3 to form NH_4NO_3 aerosols if thermodynamically favorable (Bassett & Seinfeld, 1983). Particulate NH_4NO_3 formation is thermodynamically favorable when the product of NH_3 and HNO_3 mixing ratios is supersaturated relative to the equilibrium constant K_p (i.e., $[NH_3][HNO_3] > K_p$), and K_p is exponentially lower at cooler temperatures (e.g., Kim et al., 1993; Stelson et al., 1979) and lower at higher relative humidity (RH) for aqueous aerosols (as opposed to dry) (e.g., Bassett & Seinfeld, 1983; Russell et al., 1983). The gas-aerosol partitioning of the NH_3-HNO_3-NH_4NO_3 system is further complicated by interactions of NH_4^+ with other inorganic species such as non-volatile cations (NVCs; e.g., sodium [Na^+], potassium [K^+], calcium [Ca^{2+}], magnesium [Mg^{2+}]), organic acids (e.g., formate, oxalate, acetate), and nonpolar organic compounds (e.g., levoglucosan) (e.g., Metzger et al., 2006; Pun et al., 2002), so these complex gas-aerosol systems are studied using aerosol thermodynamic models.

Previous studies have used aerosol thermodynamic models to study inorganic gas-aerosol partitioning, including NH_4^+ formation, in various settings. Two common models are the Extended Aerosol Inorganics Model (E-AIM) (Clegg et al., 1998; Friese & Ebel, 2010) and ISORROPIA II (Fountoukis & Nenes, 2007). E-AIM is considered more accurate (Hennigan et al., 2015) and explicitly solves for thermodynamic equilibrium, with options to include Na^+ and Cl^- (Friese & Ebel, 2010) and organic acids and amines (Clegg et al., 2001). In contrast, ISORROPIA II trades accuracy for computational efficiency by making several approximations and includes Na^+, K^+, Mg^{2+}, Ca^{2+}, and Cl^- and an option to use precalculated activity coefficients for even faster calculations (Fountoukis & Nenes, 2007). Both of these models can calculate NH_3-NH_4^+ and HNO_3-NO_3^- partitioning either (a) as closed-system problems by using total (gas + aerosol) concentrations as inputs to predict the equilibrium-specific aerosol and gas concentrations or (b) as open-system problems by using aerosol concentrations as inputs to predict the equilibrium gas concentrations (Pye et al., 2020). Previous studies have shown that closed-system problems can better predict aerosol pH (e.g., Fang et al., 2023; Hennigan et al., 2015; Murphy et al., 2017; Song et al., 2018; Tao & Murphy, 2019, 2021), which affects NH_3 neutralizing aerosol acidity via NH_3-NH_4^+ partitioning; thus, both gas-phase measurements of NH_3 and HNO_3 and aerosol-phase measurements are required to accurately model NH_3-NH_4^+ and HNO_3-NO_3^- partitioning. There is a large body of work that has used weekly-to-hourly measurements of gas-phase and aerosol-phase species from surface monitoring sites to study NH_3-NH_4^+ partitioning in various settings. For example, ISORROPIA II has been used to study the sensitivity of $PM_{2.5}$

to NH_3 and HNO_3 in urban and agricultural regions in the US, China, and Europe (Cheng et al., 2021; Guo et al., 2018; Nah et al., 2018) and the sensitivity of the vertical distribution of NH_3 to NH_4NO_3 partitioning at a suburban site in northeastern Colorado (Y. Li et al., 2017). E-AIM has been used to study the sensitivity of urban $PM_{2.5}$ to NH_3-NH_4^+ (Tao & Murphy, 2019, 2021), amine versus NH_3 uptake in marine $PM_{2.5}$ (Chen et al., 2022), and new approaches to estimating aerosol pH (Tao et al., 2022). However, application of these aerosol thermodynamic models to study NH_3-HNO_3-NH_4NO_3 partitioning in targeted agricultural NH_3 plumes at high sub-hour temporal resolution is lacking.

In comparison to surface monitoring sites, ground-based and airborne mobile sampling have the benefit of targeting NH_3 plumes from AFO outflow. Previous studies using ground-based mobile sampling have reported NH_3 and methane (CH_4) enhancement ratios from AFOs in northeastern Colorado (Eilerman et al., 2016) and the San Joaquin Valley in California (Miller et al., 2015). However, the inclusion of aerosol instrumentation in their payloads were restricted by space and power supply, and coverage was limited by speed and to roads. In contrast, airborne sampling provides better spatial and vertical coverage, but can share similar space/power limitations. Sorooshian et al. (2008) deployed a suite of instrumentation to characterize aerosols (e.g., composition, hygroscopicity, size distribution, etc.) downwind of an AFO but did not make any gas-phase measurements, so they could only infer whether NH_4NO_3 formation was NH_3- or HNO_3-limited. Staebler et al. (2009) measured NH_4^+, NO_3^-, SO_4^{2-}, and non-refractory organic aerosols and gaseous NH_3 (but not HNO_3) downwind of one AFO on three flights to study NH_3 loss processes. They found NH_3 loss to gas-aerosol partitioning was negligible (<4% NH_4^+:NH_x), and dominated by advection (90%) and dry deposition (10%), on their three flights but did not utilize models to parse out which thermodynamic factors were inhibiting NH_4NO_3 formation. Hacker et al. (2016) tracked NH_3 and CH_4 enhancements downwind of AFOs on seven different flights, but could only measure NH_3 and CH_4 on alternating flights due to space/weight/power limitations of the two-seat motor glider. Schobesberger et al. (2023) measured NH_4^+, SO_4^{2-}, NO_3^-, and non-refractory organic aerosols and NH_3 to investigate the surface-atmosphere exchange of NH_3 and found net NH_3 flux from the surface to the atmosphere at an agricultural region; they also note that NH_3:NH_4^+ ratios are lower in the free troposphere compared to the boundary layer likely due the temperature-dependence of NH_3-NH_4^+ partitioning. In addition to the aforementioned airborne studies that measured outflow from individual AFOs, there have been several other airborne studies that have observed NH_4NO_3 formation in regional outflow. Nowak et al. (2010) reported NH_4NO_3 formation in urban outflow over Houston when the research aircraft inadvertently intercepted NH_3 plumes from an industrial accident and an unidentifiable source. Nowak et al. (2012) presented a case study that observed favorable conditions for NH_4NO_3 formation downwind of a region of dairy farms in the California South Coast Air Basin on one flight and showed NH_4NO_3 formation could be mitigated more effectively by NH_3 reductions from dairy rather than from traffic. Franchin et al. (2018) showed reported significant NH_4NO_3 formation during winter pollution episodes in Utah and used ISORROPIA to show NH_3 and HNO_3 reductions can reduce NH_4NO_3 formation but its effectiveness varies by location between the Cache, Salt Lake, and Utah valleys.

In a 2019 pilot study to the Transport and Transformation of Ammonia ($TRANS^2Am$) campaign, Pollack et al. (2022) used 1 Hz measurements of NH_3, CH_4, and ethane (C_2H_6) to isolate agricultural CH_4 from nearby oil and natural gas (ONG) CH_4 emissions and quantify NH_3:CH_4 enhancement ratios from 6 AFOs, and McCabe et al. (2023) used these measurements to compare two methods of calculating agricultural CH_4 emission rates in a region with co-located ONG activity and reported NH_3 and CH_4 fluxes from livestock. Building off of this pilot study, the full $TRANS^2Am$ campaign included a more comprehensive payload with the addition of gas-phase HNO_3 and aerosol composition measurements and was conducted in northeastern Colorado in July/August 2021 (Phase I) and August 2022 (Phase II). The $TRANS^2Am$ campaign provides a unique data set containing both gas and aerosol composition at high temporal resolution in and around agricultural NH_3 plumes from targeted facilities, which can be used to quantify NH_3 emissions and study the near-source evolution and loss processes of NH_3 from AFOs (Juncosa Calahorrano et al., 2023).

In this work, we use the comprehensive suite of observations from Phase I of $TRANS^2Am$ in tandem with model analyses to investigate (a) the sensitivity of PM formation to AFO emissions and (b) the seasonality of NH_4NO_3 formation in northeastern Colorado. Section 2 outlines the aircraft- and ground-based observations and modeling approach used in this study. Section 3 explores the sensitivity of summertime NH_4NO_3 formation to precursor

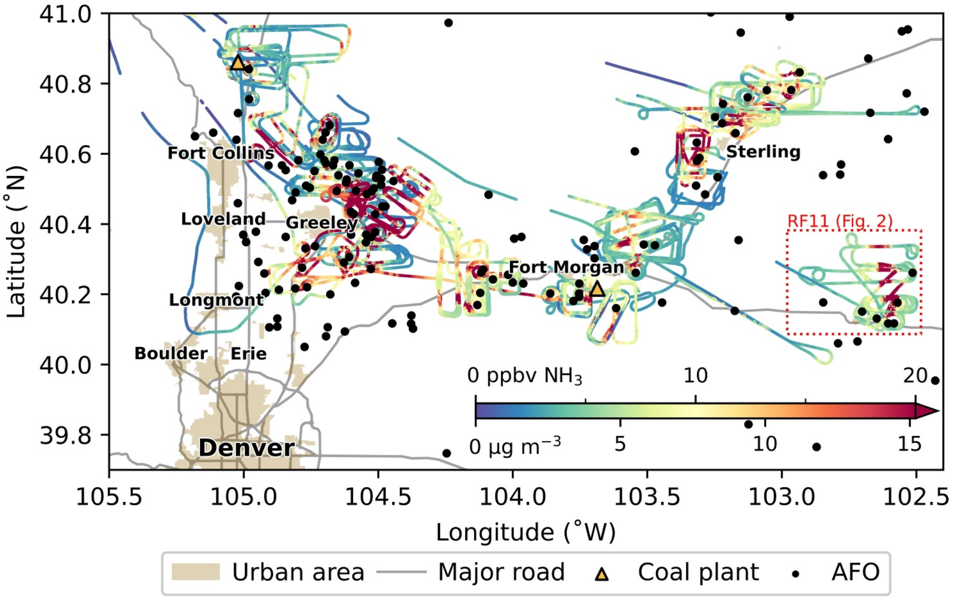

Figure 1. Map of near-source flights from TRANS^{2}Am Phase I (≤1,500 m agl) colored by 1 Hz NH_3 concentration. The colorbar is truncated at 20 ppbv, and the maximum observed NH_3 concentration is >400 ppbv. The red dotted line outlines RF11, which is plotted as a time series in Figure 2.

emissions and meteorological conditions, then predicts the seasonality of NH_4NO_3 formation by modeling idealized scenarios beyond the summertime measurements. Section 4 summarizes our findings.

2. Methods

2.1. TRANS^{2}Am

The Transport and Transformation of Ammonia (TRANS^{2}Am) campaign deployed the University of Wyoming King Air (UWKA) over northeastern Colorado (Figure 1) during July/August 2021 (Phase I) and August 2022 (Phase II) to characterize the atmospheric composition downwind of AFOs and understand the chemical and physical evolution of NH_3. There were 24 research flights consisting of 17 near-source sampling flights, 6 upslope flights, and 1 satellite-underpass. Combined with a low-altitude waiver, this smaller research aircraft was able to routinely sample between approximately 60 and 300 m agl. Here we focus on the inorganic gas-aerosol partitioning during only the Phase I near-source sampling flights. Near-source sampling flights included circling facilities to manually identify the outflow direction, followed by vertically stacked boxes at multiple intervals downwind of targeted AFOs. Flights were generally flown on hot, dry afternoons when surface winds were strong (>5 m s^{-1}) enough to form and identify well-defined NH_3 plumes. Smoke-impacted days accounted for 8 of the 10 near-source sampling flights during Phase I in 2021.

Figure 1 shows the study region including a large number of different types of AFOs (e.g., cattle, dairy, poultry, etc.), and urban areas along the major road corridor from Denver to Fort Collins. Active oil and gas operations in this region are depicted in Pollack et al. (2022). The study region is bordered by the Rocky Mountains on the west. We restrict the analysis to data collected below 1,500 m agl and ≤41°N. This removes data associated with takeoff/landing from the operations base at Laramie Regional Airport.

2.2. Aircraft Instrumentation

The UWKA instrument payload measured a suite of aerosol-phase and gas-phase species to study the inorganic gas-aerosol partitioning around AFO outflow. The full instrument payload is described in detail in Juncosa Calahorrano et al. (2023), so here we describe the payload relevant to our study and summarize it in Table 1.

Table 1

Summary of University of Wyoming King Air Instrument Payload and Measured Parameters Used in This Work

Parameter	Instrument	Sampling frequency	Limit of detection
Submicron aerosol composition	PILS with fraction collector	2 min	0.001 μg m^{-3}
NH_4^+			0.001 μg m^{-3}
SO_4^{2-}			0.001 μg m^{-3}
NO_3^-			0.001 μg m^{-3}
NO_2^-			0.001 μg m^{-3}
Cl^-			0.001 μg m^{-3}
Na^+			0.001 μg m^{-3}
K^+			0.001 μg m^{-3}
Mg^{2+}			0.001 μg m^{-3}
Ca^{2+}			0.001 μg m^{-3}
Formate $HCOO^-$			0.001 μg m^{-3}
Acetate CH_3COO^-			0.001 μg m^{-3}
Oxalate $C_2O_4^{2-}$			0.001 μg m^{-3}
Propionate $C_3H_5O^{2-}$			0.001 μg m^{-3}
MSA[a] $CH_3SO_3^-$			0.001 μg m^{-3}
Succinate $C_4H_4O_4^{2-}$			0.001 μg m^{-3}
Glutarate $C_5H_7O_4^-$			0.001 μg m^{-3}
Levoglucosan $C_6H_{10}O_5$			0.001 μg m^{-3}
NH_3	QC-TILDAS operating at 967 cm^{-1}	1 s	180 pptv
HNO_3	QC-TILDAS operating at 1,723 cm^{-1}	1 s	555 pptv

[a] Methanesulfonate (MSA).

Figure 2 shows an exemplary time series of the full suite of observations collected during a single research flight on 17 August 2021. The full suite of observations includes 9 inorganic species, 8 organic species, and gas-phase NH_3 and HNO_3. The NH_3 and HNO_3 measurements are averaged from 1 Hz to 2 min in order to match the time resolution of the PILS measurements. The 2 min averaged NH_3 masks much of the observed high frequency variability present in the 1 Hz observations. For instance, the reported maximum gas-phase NH_3 reported here (114 ppbv) corresponds to the 2-min average, whereas the maximum NH_3 sampled using the 1 Hz data is >400 ppbv. Temperature, RH, and geospatial data are from the UWKA standard suite of instrumentation.

Water-soluble aerosol samples were collected by a Particle-into-Liquid Sampler (PILS) with a fraction collector for offline analysis using ion chromatography. A PILS works by collecting ambient aerosol particles into pure water to produce a liquid sample with aerosol particles dissolved in it. The PILS sampled air at 15 LPM from the NCAR-University of Wyoming Aerosol Inlet mounted on top of the UWKA fuselage (Snider et al., 2018). A non-rotating MOUDI impactor stage upstream of the PILS removes super-micron particles to provide a size cutoff of 1 μm (PM_1) (Marple et al., 1991). Sodium-carbonate- and phosphorous-acid-coated denuders remove gaseous interference before the particles are mixed with hot steam to create a supersaturated environment (RH ≥ 100%) and grow the particles large enough to be collected by an impactor. The particles are then washed off the impactor by a continuous flow of deionized water providing the liquid sample with the dissolved aerosol particles for analysis (Orsini et al., 2003). Finally, the liquid sample is continuously collected by a Bretchel Fraction Collector for offline analysis (Sorooshian et al., 2006). The fraction collector holds seventy-two 2 mL polypropylene vials on a carousel, and the PILS liquid flow rate was set such that a ~1.2 mL liquid sample is collected into a vial every 2 min (Sullivan et al., 2022). Preloaded carousels were manually switched during each flight to allow for collection of samples across an entire flight. Background samples were also collected each flight for 10 min by forcing the airflow through a HEPA filter before entering the PILS. Immediately after each flight, the vials were unloaded, recapped with solid caps, and transported to Colorado State University in coolers with ice packs to be stored at 2°C until analysis.

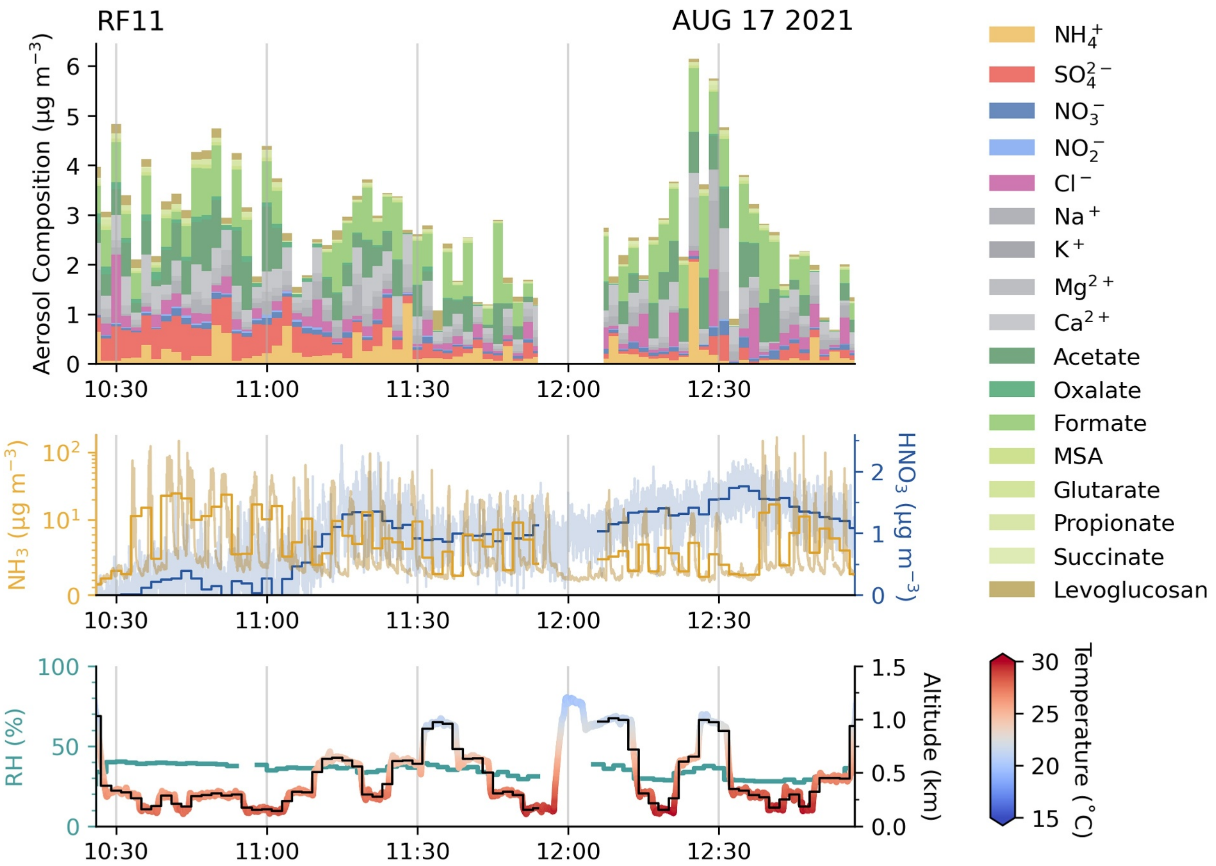

Figure 2. Time series of observations from RF11 in local time. The flight track from RF11 is outlined by the red dotted line in Figure 1 and the plane is flying vertically stacked boxes as it moves downwind of the target facility from ~10:30 to 12:30 before flying back south and circling the target facility again. Top: Aerosol-phase measurements colored by species. Middle: Gas-phase NH_3 in yellow (left *y*-axis) and HNO_3 in blue (right *y*-axis) averaged to 2-min Particle-into-Liquid Sampler timesteps. Light shade represents native 1 Hz measurements. Bottom: RH (left *y*-axis) and altitude colored by temperature (right *y*-axis). See Table S1 in for summary statistics of each species.

Offline analysis of PILS samples was performed by ion chromatography to determine the aerosol-phase concentrations of cations, anions/organic acids, and levoglucosan (full list of species measured provided in Table 1). Cations were determined using a Dionex ICS-3000 ion chromatography with a pump, conductivity detector, and self-regenerating cation suppressor. A Dionex IonPac CS12A-5 μm analytical column (3 × 150 mm) using 20 mM methanesulfonic acid manually made at a flow rate of 0.5 mL/min was used for the cation separation. The injection volume and analysis time were 190 μL and 17 min, respectively. Anions/organic acids were measured using a Dionex ICS-4000 capillary ion chromatograph, which includes an eluent generator, isocratic pump, degausser, suppressor, carbonate removal device, and conductivity detector. A Dionex AS11-HC capillary column with a potassium hydroxide (KOH) gradient provided by the eluent generator at a flow rate of 0.015 mL/min was used for the separation. The complete run time was 65 min with a separation method as follows: (a) 13 min isocratic elution with 1 mM KOH, (b) 20 min linear gradient from 1 to 15 mM KOH, (c) 10 min linear gradient from 15 to 30 mM KOH, (d) 5 min linear gradient from 30 to 45 mM KOH, and (e) 17 min re-equilibration step to return to the starting conditions. An injection volume of 35 μL was used. Levoglucosan was determined via high-performance anion-exchange chromatography with pulsed amperometric detection using a Dionex DX-500 series ion chromatograph with an ED-50/ED-50A electrochemical cell. The cell includes two electrodes: a pH-Ag/AgCl (silver/silver chloride) reference electrode and "standard" gold working electrode. For the separation, a Dionex CarboPac PA-1 column (4 × 250 mm) employing a sodium hydroxide gradient was used. The complete run time was 59 min, and the injection volume was 100 μL. More details on the method can be found in Sullivan, Frank, Onstad et al. (2011), Sullivan, Frank, Kenski, and Collett (2011), and Sullivan et al. (2014, 2019, 2022). Samples were blank-corrected using the average of all background samples collected on that particular flight. The uncertainty is ±10% and the limit of detection is 0.001 μg m^{-3} for all species.

NH_3 mixing ratios were measured using a closed-path quantum-cascade tunable infrared laser direct absorption spectrometer (QC-TILDAS) with an effective path length of 76 m and operating at 967 cm^{-1} (Ellis et al., 2010; McManus et al., 1995, 2010; Zahniser et al., 1995). The details of the flight-ready NH_3 instrument are reported in Pollack et al. (2019). The aircraft injection inlet and inertial inlet system shared by the NH_3 and HNO_3 instrument in this work are configured and operated in a similar manner as reported in Pollack et al. (2019). Briefly, the NH_3 QC-TILDAS is operated with a high sample flow rate (>10 SLPM) to help prevent adsorption of NH_3 to the sampling surfaces. The instrument was also operated with a 40 ± 2°C heated inertial inlet positioned along the flowpath to reduce (a) condensation of water (that NH_3 can dissolve in/adsorb to), (b) adsorption of NH_3 to the sampling surfaces, and (c) a positive bias from semivolatile ammonium particles >300 nm in diameter (Ellis et al., 2010). The time response of the NH_3 QC-TILDAS has been previously characterized and defined as the time required for 90% signal recovery following a step change in NH_3 calibration signal (Pollack et al., 2019). During $TRANS^2Am$, a time response of 1–2 s without surface passivation could be maintained by regularly cleaning the instrument sampling surfaces between flights. The instrument was calibrated on the ground between flights and regularly zeroed in flight by overblowing the aircraft inlet with ultra-pure air. The flowpath was also copiously flushed with ultra-pure air following calibrations. The calibration source was a thermally-stabilized, certified NH_3 permeation device (Kin-Tek). The permeation rate of the calibration source was verified before and after the field study using the NOAA UV absorption system and determined to have an uncertainty of ±10% (Neuman et al., 2003; Pollack et al., 2019). The instrument was also mounted on a vibrationally-isolated rack to minimize motion sensitivity in flight (Pollack et al., 2019). The 1-Hz precision of the instrument is 60 pptv; the detection limit is defined as three times the precision (180 pptv). NH_3 measurements are collected at 10 Hz and averaged to 1 Hz for reporting and further averaged to 2 min to match the PILS time resolution for this analysis. The uncertainty of NH_3 is ±12% of the measured mixing ratio (Pollack et al., 2019).

HNO_3 mixing ratios are measured using a separate closed-path QC-TILDAS with a 76 m pathlength and measuring absorption by the molecule at 1,723 cm^{-1} (Roscioli et al., 2016). Owing to weight, space, and power available on the UWKA, the HNO_3 measurements were categorized as second priority for the $TRANS^2Am$ payload. The only way the HNO_3 QC-TILDAS could be implemented aboard the aircraft was to share a common aircraft inlet, inertial inlet, and pumping system with the NH_3 instrument. Because of the shared flowpath, the same instrument operation practices are applied (e.g., regular in-flight zeros, calibrations on the ground between flights, regularly cleaning samping surfaces and inlet components, and copiously flushing the sample flow path with ultrapure air following individual NH_3 and HNO_3 calibrations). The HNO_3 QC-TILDAS is also mounted on vibration isolators in the aircraft equipment rack. The 1-Hz precision is 185 pptv resulting in a detection limit of 555 pptv. The uncertainty for the HNO_3 measurement is determined to be ±20% of the measured mixing ratio following the procedures in Pollack et al. (2019). When operated with a dedicated flowpath, the HNO_3 QC-TILDAS has been previously reported to have a 70 s time response for a 90% signal recovery (Roscioli et al., 2016). Even with the high sample flow rate (>10 SLPM) and regular cleaning of the sampling surfaces, the 90% HNO_3 signal recovery time following a step change in HNO_3 calibration signal during ground calibration days between flights during $TRANS^2Am$ was closer to 500 s. The longer response time is likely related to the HNO_3 QC-TILDAS being positioned downstream of the NH_3 QC-TILDAS. There was a longer flow path between the inlet tip and the HNO_3 detector, and this pathway was susceptible to adsorption of HNO_3 on the sampling surfaces prior to detection. Owing to a larger detection limit and uncertainty in the HNO_3 measurement compared to NH_3, we consider the $1/e$ response time (which is closer to 200 s) to be a more representative time response for the HNO_3 measurement. For this work, and to match the sampling frequency of PILS, the HNO_3 measurements are averaged to 120 s prior to further analyses.

Active continuous passivation of the sampling surfaces has been shown to improve time response for closed-path QC-TILDAS instruments (Pollack et al., 2019; Roscioli et al., 2016). Prior work shows success in improving the time response of a single-channel, closed-path NH_3 QC-TILDAS when using a strong perfluorinated base as the passivant and for a separate HNO_3 QC-TILDAS when using a strong perfluorinated acid as the passivant (Pollack et al., 2019; Roscioli et al., 2016). However, active continuous passivation could not be implemented during $TRANS^2Am$ owing to the common flow path for the payload configuration.

2.3. Model

Extended Aerosol Inorganic Model (E-AIM) was used to investigate factors driving the gas-aerosol partitioning of NH_3 and HNO_3. The E-AIM Model II (http://www.aim.env.uea.ac.uk/aim/aim.php) calculates the equilibrium phase partitioning of an inorganic H_2O-SO_4^{2-}-NO_3^--NH_4^+ aerosol system with an option to add preset and custom organic acids and amines. In this study, we add the three most abundant organic acids–formic acid, oxalic acid, and acetic acid–to the default inorganic aerosol system with custom property files that include molar mass, dissociation constants (https://pubchem.ncbi.nlm.nih.gov/, last accessed 28 February 2024), UNIFAC activity coefficients, and Henry's Law constants (Sander, 2023) and restrict the organic compounds to the aqueous-phase. The model inputs are measurements of temperature, relative humidity, total ammonia ($NH_x = NH_3 + NH_4^+$), and total nitrate ($TNO_3 = HNO_3 + NO_3^-$), as well as particle-phase sulfate, formate, acetate, and oxalate. The primary model outputs used in our study are the equilibrium gas-aerosol partitioning of total NH_x and TNO_3. To apply E-AIM to our analysis, we make a key assumption that the submicron aerosol population is internally mixed and at metastable equilibrium.

2.3.1. Internally Mixed Assumption

Aerosols are likely not truly internally mixed in the real atmosphere (e.g., Riemer et al., 2019), so we conduct a comprehensive suite of sensitivity tests with varying combinations of model input species to best represent the aerosol composition undergoing NH_3-HNO_3-NH_4NO_3 partitioning (Figure S1 in Supporting Information S1). We find that the inclusion of formate, oxalate, and acetate in the model help correct for NH_4^+ and NO_3^- underestimates by the model (Figures S1a and S1b in Supporting Information S1), and these three compounds have been observed to be the most abundant organic acids in aerosols (Nah et al., 2018). The predicted equilibrium vapor pressure of oxalic acid ranges from pptv to ppbv and is relatively low as it is predicted to be mostly dissociated in the particle phase. In contrast, the predicted equilibrium vapor pressures of acetic and formic acid ranges from tenths to tens of percent, and they are predicted to be mostly undissociated in the particle phase. The equilibrium gas-phase concentrations of acetic and formic acid are unrealistically high compared to the tens of ppbv or less reported in wildfire plumes (Permar et al., 2023) and the <0.1% total mixing ratio of trace gases in dry air, but the reason for this is unclear and beyond the scope of this study. We find that the inclusion of NVCs and Cl^- causes E-AIM to overpredict NO_3^- on aggregate, suggesting that NVCs are externally mixed (or associated with unmeasured carbonate ions) (Section S1, Figures S1e and S1f in Supporting Information S1), so we do not include NVCs in our model for analysis. We also find that the inclusion of levoglucosan, a moderate polar organic compound (Petters & Kreidenweis, 2007), and a proxy for unmeasured smoke-related organic compounds (Section S1, Figures S2 and S3 in Supporting Information S1) worsens model-observation agreement (Figure S1 in Supporting Information S1).

2.3.2. Equilibrium Assumption

Previously, it has been shown that submicron aerosols can reach equilibrium within minutes to a few hours (Meng & Seinfeld, 1996). We do not calculate plume age and the time to reach equilibrium, so the equilibrium assumption is ultimately a shortcoming of this study given the strong perturbations of NH_3 in AFO plumes and may contribute to overestimates in modeled NH_4NO_3. We identify two conditions of nonequilibrium behavior in 9% of our data (Section 3.3).

2.3.3. Metastable Equilibrium Assumption

Previous studies ran E-AIM and ISORROPIA II in metastable mode (e.g., Cheng et al., 2021; Guo et al., 2018; Nah et al., 2018; Tao & Murphy, 2019, 2021; Tao et al., 2022) because aqueous aerosol salts have been observed in the atmosphere below their deliquescence relative humidity (DRH) and above their crystallization relative humidity (CRH) (Rood et al., 1989), so we also run the model in metastable mode such that aerosols may exist in the aqueous phase below their DRH. The observed RH is above the DRH of NH_4NO_3 and $(NH_4)_2SO_4$ in approximately 30% and 6% of observations, respectively, and above the CRH of $(NH_4)_2SO_4$ in approximately 44% of observations. No CRH is observed for NH_4NO_3 (Davis et al., 2015). The presence of organics has also been shown to lower the CRH of $(NH_4)_2SO_4$ (e.g., Choi & Chan, 2002; Pant et al., 2004), which would allow aerosols to exist in a metastable state at even lower ranges of RH. We find improved modeled gas-aerosol partitioning when assuming metastable equilibrium as opposed to stable equilibrium (Figure S4 in Supporting Information S1).

2.4. Integrated Ground-Based Measurements

We also include gas-phase HNO_3 and NH_3 measurements from a ground-based URG annular denuder/filter pack sampler located at the Weld County Tower site in Greeley, Colorado, which is operated by the Colorado Department of Public Health and Environment (CDPHE). Weekly samples were collected from mid-March through mid-October from 2014 to 2019 (but not 2018). Ambient air was pulled into the sampler at a flow rate of 3 LPM through a $PM_{2.5}$ Teflon-coated cyclone followed by sodium carbonate and phosphorous acid coated denuders to collect gas-phase HNO_3 and NH_3 (Benedict, Chen, et al., 2013). The air then passed through a 47 mm nylon filter to collect PM. Finally, the air passed through a second phosphorous acid denuder to collect any particulate NH_4^+ that volatilized off the filter. The nylon filter efficiently retains volatilized nitric acid (Yu et al., 2005).

Each nylon filter was extracted in 6 mL DI Water in a polystyrene test tube and sonicated without heat for 40 min. Each denuder was extracted in 10 mL DI Water. Both extracts were then analyzed for anion and cation species using ion chromatography. Both systems utilized a Dionex DX-500 IC, which includes an isocratic pump, self-regenerating anion or cation suppressor, and conductivity detector. The anions were quantified using a Dionex IonPac AS14A (4 × 150 mm) analytical column using a manually made eluent mixture of 1 mM sodium bicarbonate and 8 mM sodium bicarbonate at a flow rate of 1 mL/min. A Dionex IonPac CS12A-5 μm (3 × 120 mm) analytical column was used with 20 mM methanesulfonic acid eluent manually made at a flow rate of 0.5 mL/min. The injection volume and analysis time of both methods was 50 μL and 17 min, respectively.

3. Results

3.1. Overview

Figure 1 shows that northeastern Colorado is characterized by high and spatially variable NH_3 concentrations. NH_3 concentrations have been shown to vary by orders of magnitude from tens of pptv over remote oceans to tens of ppbv in agricultural regions (Nair & Yu, 2020), and can exhibit steep spatial gradients within agricultural regions (Benedict, Day, et al., 2013). Y. Li et al. (2017) reported weekly and biweekly averaged NH_3 concentrations at 14 surface monitoring sites in northeastern Colorado during summers 2010–2015 ranging from 4 ppbv (2.66 μg m^{-3}) over grasslands to 60 ppbv (42.7 μg m^{-3}) near AFOs. Due to the finer temporal resolution and the spatial and vertical variability of our airborne measurements, we capture higher concentrations (20–114 ppbv) in targeted AFO outflow and lower concentrations outside of plumes (0.5–20 ppbv). We found that NH_3 accounts for 93% of NH_x on average, and Day et al. (2012) also found that NH_x is dominantly in the gas-phase throughout the year in northeastern Colorado.

HNO_3 concentrations observed during TRANS^{2}Am demonstrate much less spatial and temporal variability than NH_3 concentrations. HNO_3 concentrations were 1.7 ppbv on average and varied from below LOD (555 pptv) to 4 ppbv, and accounted for about 94% of TNO_3 on average. We did not identify any spatial gradients of increasing HNO_3 concentrations toward urban areas, although the UWKA did not sample directly over urban areas.

For the species that the PILS resolves in this study, PM_1 concentrations were 4.8 μg m^{-3} on average ($\sigma = 2.0$ μg m^{-3}), with inorganic species accounting for 54% by mass and 66% by moles and organic species accounting for 45% by mass and 33% by moles. The observed inorganic PM_1 mass is dominated by sulfate (0.52 ± 0.37 μg m^{-3} [mean ± standard deviation]), nitrate (0.33 ± 0.48 μg m^{-3}) and ammonium (0.38 ± 0.54 μg m^{-3}). The observed organic PM_1 mass is dominated by acetate (1.1 ± 0.7 μg m^{-3}), formate (0.72 ± 0.61 μg m^{-3}), and oxalate (0.14 ± 0.13 μg m^{-3}).

3.2. Observed Thermodynamic Regimes

Figure 3 shows that the thermodynamic regimes sampled during TRANS^{2}Am are always NH_3-rich and mostly HNO_3-limited. The thermodynamic regimes are determined by the gas ratio, which was introduced by Ansari and Pandis (1998) and is defined in molar concentrations:

$$\text{Gas Ratio} = \frac{\text{Free Ammonia}}{\text{Total Nitrate}} = \frac{[NH_x] - 2[SO_4^{2-}]}{[TNO_3]} = \frac{[NH_3] + [NH_4^+] - 2[SO_4^{2-}]}{[TNO_3]}$$

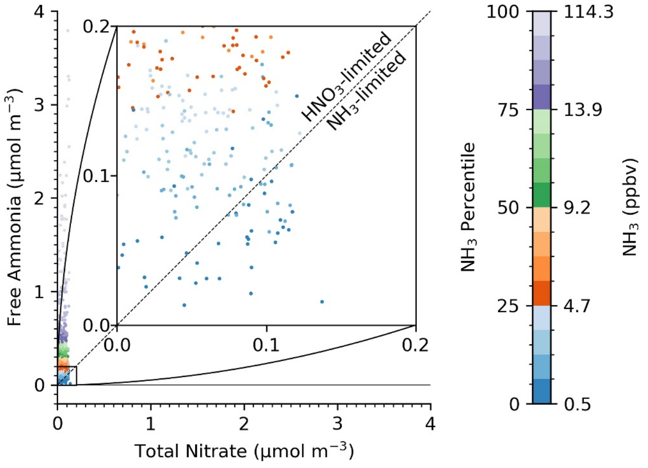

Figure 3. Molar concentrations of free ammonia ($NH_3 + NH_4^+ - 2SO_4^{2-}$) versus total nitrate ($HNO_3 + NO_3^-$). Colorbar represents NH_3 percentiles and respective concentrations in ppbv are given for quartiles. Inset axes are zoomed in to the range of observed total nitrate. The dashed line delineates NH_3- and HNO_3-limited NH_4NO_3 formation regimes.

The gas ratio is always positive, indicating that sulfate is always fully neutralized and that there is always sufficient NH_3 and HNO_3 to form NH_4NO_3. Only 6% (37/629) of sample air masses have a gas ratio between 0 and 1 where NH_4NO_3 formation is NH_3-limited; the remaining 94% (592/629) have a gas ratio greater than 1, where NH_4NO_3 formation is HNO_3-limited. NH_3-limited conditions are only measured when NH_3 is in the lowest 25th percentile (≤4.7 ppbv). These conditions only occur sporadically away from major sources. Even though summertime AFO outflow is largely HNO_3-limited, NH_4NO_3 formation can still be sensitive to NH_3 (Section 3.4).

3.3. Thermodynamic Modeling

Figure 4 shows the distribution of observed and modeled NH_4^+ and NO_3^- binned by altitude. We find that across the full campaign in aggregate, the E-AIM simulations capture the correct order of magnitude of the observed NH_4^+ and NO_3^- concentrations. Model and observations agree that there was generally little NH_4NO_3 formation, especially below 300 m. Below 300 m agl, NH_4^+ exceeds 1 µg m^{-3} only 2% of the time in observations and 0.3% of the time in the model, and NO_3^- exceeds 1 µg m^{-3} 4% of the time in observations and 3% of the time in the model. Summertime Colorado is hot and dry, both of which thermodynamically inhibit NH_4NO_3 formation and drive gas-aerosol partitioning into the gas-phase.

A variance analysis reveals that E-AIM systematically underpredicts NH_4^+ by 102% and NO_3^- by 72% of the measured mass concentration (Figures S5c and S5h in Supporting Information S1) when excluding samples from two non-equilibrium conditions we identified. The model overpredicts NH_4^+ and NO_3^- under two different non-equilibrium conditions: (a) when the plane samples in extremely concentrated AFO plumes with NH_3 concentrations >50 ppbv (Figures S5a and S5e in Supporting Information S1) in 3% (20/642) of our observations and (b)

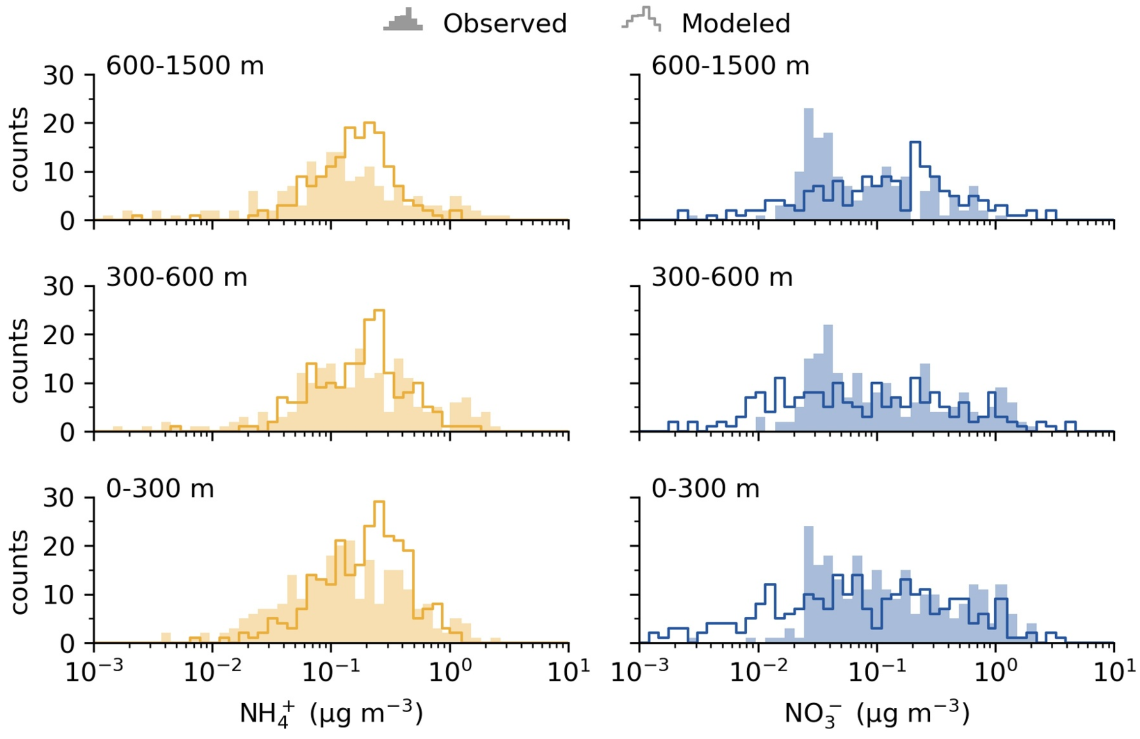

Figure 4. Distributions of observed (shaded region) and modeled (solid line) NH_4^+ (left) and NO_3^- (right) by altitude bins (rows) for the 10 near-source flights during TRANS²Am Phase I.

when the plane ascends to cooler temperatures (<20°C) under high-HNO_3 (>2 ppbv) conditions (Figures S5e and S5f in Supporting Information S1) in 6% (39/642) of our observations. The first non-equilibrium condition occurs mostly on one flight (RF13) which sampled the highest NH_3 concentrations by almost an order of magnitude (Figure S6 in Supporting Information S1), suggesting that the NH_3-HNO_3-NH_4NO_3 system was supersaturated with NH_3 and did not yet reached equilibrium. The second non-equilibrium condition occurs mostly on two post-precipitation flights (RF02 and RF12) which sampled on the 2nd and 3rd coolest days duringTRANS^{2}Am (Figure S7 in Supporting Information S1). Cool, high-HNO_3 conditions favors gas-aerosol partitioning to the aerosol phase; however, the time to reach equilibrium significantly increases from <1 min for liquid particles to >>10 min for solid/semi-solid particles due to kinetic mass transfer limitations imposed by low-viscosity particle-phase organics (Liggio et al., 2011), and TRANS^{2}Am generally sampled under dry conditions when particles may be solid/semisolid. We find worsened model-observation agreement in E-AIM at RH <40% (Figures S8 and S9 in Supporting Information S1), similar to a previous work that used ISORROPIA to study HNO_3-NO_3^- partitioning (Guo et al., 2016). These results suggest E-AIM might be correct in predicting NH_4NO_3 formation is favorable under the observed cool, dry, high-HNO_3 conditions, but its instantaneous equilibrium assumption may be unsuitable for application to observations made in concentrated AFO plumes or cool, dry conditions and result in the overprediction of NH_4^+ and NO_3^-. Due to these various limitations, we are unable to draw conclusions about individual plumes, and we restrict the interpretation of our analysis to the data on aggregate and on individual flights.

3.3.1. Case Study 1: Cool and Humid Conditions (RF08)

Figure 5 shows a time series of observed as well as modeled aerosol species concentrations (Figure 5a) and meteorological parameters (Figure 5b) for RF08 on 13 August 2021 in the context of the entire campaign (Figures 5c–5e). Figure 5a shows the nanoequivalents (i.e., nmol m^{-3} × ion charge such that 1 nmol m^{-3} = 1 neq m^{-3} for NH_4^+ and NO_3^-, and 1 nmol m^{-3} = 2 neq m^{-3} for SO_4^{2-}) of modeled and observed cations and anions, and the model captures the temporal trends of both NH_4^+ and NO_3^-, replicating NH_4^+ and NO_3^- well ($r = 0.52$ for NH_4^+ and $r = 0.88$ for NO_3^-), with generally higher concentrations observed in the first half of the flight and lower concentrations in the second half. Compared to all other flights of Phase I of TRANS^{2}Am, this flight had exceptionally cool, humid conditions, and higher observed NO_3^-. RH is consistently >60% throughout RF08 (Figure 5e); 60% is an approximate threshold above which spontaneous water uptake occurs and further favors the partitioning of NH_x and TNO_3 into the particle-phase (Wexler & Seinfeld, 1991). RF08 also has the coolest temperature conditions encountered during the campaign, with a surface temperature near 20°C rather than ~30°C for most other flights (Figure 5e inset). The uncharacteristically cool, humid conditions may be partially explained by the flight time since RF08 was conducted in the morning (~9:00–11:30), as opposed to most other flights conducted in the early afternoon. There are no precipitation events on this day or the day before, thus illustrating a diurnal temperature-driven variability that favors NH_4NO_3 formation during cool, low-TNO_3 morning hours and inhibits NH_4NO_3 formation during warm, high-TNO_3 midday and early evening hours (Figure S10 in Supporting Information S1), despite diurnal peaks in NH_3 emissions (Juncosa Calahorrano et al., 2023) and HNO_3 concentrations (Lindaas et al., 2017). Observed NO_3^- on RF08 is approximately three times higher than the average over the entire campaign (Table S1) and accounts for 50% of observed NO_3^- greater than 1 μg m^{-3}. High TNO_3 is favorable for NH_4NO_3 formation; however, TNO_3 on RF08 is the lowest amongst all flights (Figure S6 in Supporting Information S1), so TNO_3 concentrations did not drive NH_4NO_3 on RF08. Sensitivity tests show that NH_4NO_3 formation is much more sensitive to temperature (Section 3.4) than relative humidity (Figure S11 in Supporting Information S1). This implies cool temperatures drove NH_4NO_3 formation on RF08, and warm temperatures likely inhibited NH_4NO_3 formation on all other flights.

HNO_3 measurements for this flight did not pass quality control. Our model calculations conservatively assume that HNO_3 did not contribute to the TNO_3 input to the model because preliminary measurements of HNO_3 were very low (mean = −1.1 ppbv) and below the zero signal. As the model generally predicts the correct amount of NO_3^- during this flight, this corroborates our assumption that HNO_3 contributed trivially to TNO_3.

3.3.2. Case Study 2: Warm and Dry Conditions (RF02)

Figure 6 shows the same time series and scatter plots as in Figure 5 but for RF02 on 4 August 2021. RF02 is emblematic of many of the flights conducted on dry, warm conditions in the early afternoon during Phase I of TRANS^{2}Am, even though it occurred after a precipitation event and has the third coolest temperature profile

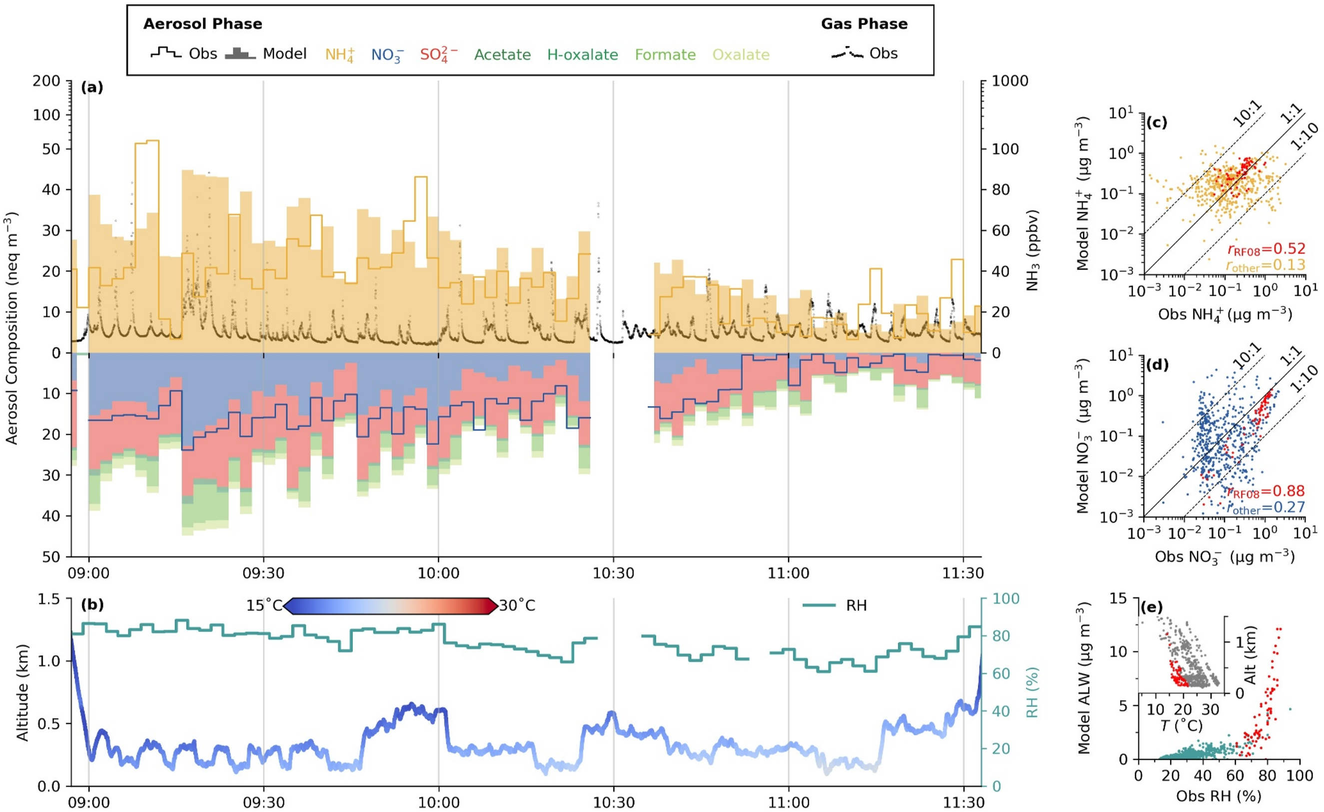

Figure 5. Time series of model and observations for RF08 (left) and model versus observations comparisons of RF08 and all other flights (right). (a) Observed (stepped lines) and modeled (shaded bars) represent aerosol composition (color) in nanoequivalents per cubic meter (neq m^{-3}) on the left *y*-axis and gas phase measurements (black dots) in ppbv on the right *y*-axis. At STP (273.15 K and 1 atm), 1 ppbv ≈ 45 nmol m^{-3} ≈ 2.8 μg m^{-3} ≈ 0.75 μg m^{-3} NH_3. (b) Time series of altitude colored by temperature on the left *y*-axis and relative humidity on the right *y*-axis. (c) Modeled versus observed NH_4^+ and *r*-value for RF08 in red and all other flights in yellow. Lines represent 10:1, 1:1, and 1:10, as labeled. *R*-values for each (d) Same as (e), except for NO_3^- and other flights are blue. (e) Modeled aerosol liquid water versus observed relative humidity for RF08 in red versus all other flights in green. Inset axes show temperature profile for RF08 versus all other flights. Note HNO_3 data is missing on RF08.

(Figure S7 in Supporting Information S1). NH_4NO_3 formation appears to be generally inhibited by hot temperatures in summertime northeastern Colorado. Temperatures were warm (20–25°C) close to the surface (<200 m agl) throughout the afternoon, and RH was largely <60%, where aerosol water uptake is limited to 2.5 μg m^{-3} or less. RF02 is one of 3 flights (also RF12 and RF13) where observed total nitrate is dominantly in the aerosol-phase in the first half of the flight and then dominantly in the gas-phase in the second half of the flight. Under these conditions, the model is able to capture the range of observed NH_4^+ and NO_3^-, but not the temporal variability ($r = 0.24$ and $r = -0.21$ for NH_4^+ and NO_3^-, respectively).

In Figure 6, NH_4^+ observations range from 10^{-3} to 10^1 μg m^{-3}, but the model only predicts NH_4^+ between 10^{-1} and 10^0 μg m^{-3}. This is possibly because the 2-min resolution is too coarse to capture the sub-2-min plume transect time and NH_3 variability. Model underestimates of NH_4^+ may also be attributable to unmeasured anions because the model assumes a neutral charge balance between cations and anions, and this work joins a growing body of literature reporting excess NH_4^+ (NH_4^+ not associated with NO_3^- and SO_4^{2-}). Schlag et al. (2017) attributed excess ambient PM_1 NH_4^+ in an agricultural region to organic acids, which can be enhanced by clouds and smoke. Di Lorenzo et al. (2018) also reported excess ambient PM_1 NH_4^+ and amines in aged smoke, even when accounting for NVCs and organic acids. Excess NH_4^+ has also been reported to be increasing with total organic carbon in long-term cloud water monitoring, suggesting NO_3^- and SO_4^{2-} are no longer sufficient to explain NH_4^+ in cloud water (Lawrence et al., 2023). Although the UWKA avoided sampling clouds during TRANS2Am, data on 8 of the 10 flights used in this study were collected on smoke-impacted days, so we conduct sensitivity tests to examine the influence of smoke on the modeled NH_3-HNO_3-NH_4NO_3 partitioning (Section S1 in Supporting Information S1). In short, when the three most abundant organic acids in the atmosphere (formate,

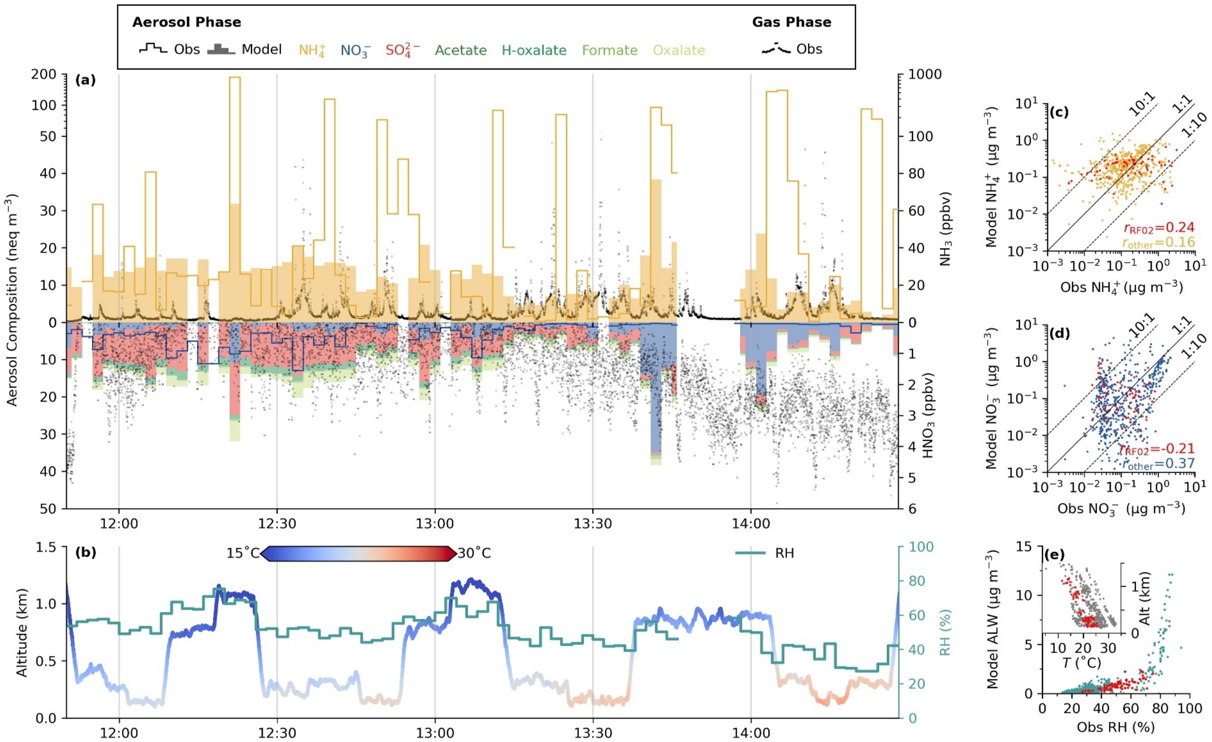

Figure 6. Time series of model and observations for RF02 (left) and model versus observations comparisons of RF02 and all other flights (right). (a) Observed (stepped lines) and modeled (shaded bars) represent aerosol composition (color) in nanoequivalents per cubic meter (neq m^{-3}) on the left *y*-axis and gas phase measurements (black dots) in ppbv on the right *y*-axis. At STP (273.15 K and 1 atm), 1 ppbv ≈ 45 nmol m^{-3} ≈ 2.8 μg m^{-3} NH_3 and 0.75 μg m^{-3} HNO_3. (b) Time series of altitude colored by temperature on the left *y*-axis and relative humidity on the right *y*-axis. (c) Modeled versus observed NH_4^+ and *r*-value for RF02 in red and all other flights in yellow. Lines represent 10:1, 1:1, and 1:10, as labeled. *R*-values for each (d) Same as (e), except for NO_3^- and other flights are blue. (e) Modeled aerosol liquid water versus observed relative humidity for RF02 in red versus all other flights in green. Inset axes show temperature profile for RF02 versus all other flights.

oxalate, and acetate) are included in the mode input, the distributions of NH_4^+ and NO_3^- shift toward higher concentrations to better match observations (Figures S1a and S1b in Supporting Information S1). Further sensitivity tests with a proxy for unmeasured organics added to the model input does not show improved model-observation agreement in NH_4^+ and NO_3^- (Figures S1c and S1d in Supporting Information S1), indicating unmeasured non-dissociating hydrophilic organics from smoke is likely not a major contributor to the NH_4^+ underprediction in E-AIM.

Figure 6 also shows an example of non-equilibrium behavior driving the model overprediction NH_4^+ and NO_3^- when ascending to lower temperatures aloft in the second half of the flight (13:40–14:05) when HNO_3 increases above ∼2 ppbv and RH remains <60%. As discussed previously in Section 3.3, this is likely a result of non-equilibrium behavior driven by slow kinetic mass transfer in dry solid/semi-solid aerosols. Although for scenarios like this, the model does not consistently capture the temporal variability of NH_3-NH_4^+ and HNO_3-NO_3^- partitioning, the model is able to consistently capture the range of NH_4^+ and NO_3^- in aggregate across the campaign (Figure 4).

3.4. Temperature-Sensitivity of Gas-Aerosol Partitioning During TRANS^{2}Am

Figure 7 shows the modeled effect of temperature and NH_x on gas-aerosol partitioning in and out of AFO plumes, and we find inorganic gas-aerosol partitioning is especially sensitive to temperature and NH_x during TRANS^{2}Am. In this simple water-SO_4^{2-}-NO_3^--NH_4^+ system with no organics or other inorganics, TNO_3, SO_4^{2-}, and RH are set to the average observed values during TRANS^{2}Am. The formation of NH_4NO_3 is inhibited by low NH_x and/or warm temperatures in the light pink region and driven by high NH_x and/or cool temperatures in the dark blue region. Between these two regimes, the formation of NH_4NO_3 is determined by a balance between temperature and NH_x. The range of observed NH_x and temperature is marked by the black outline, and observations are either

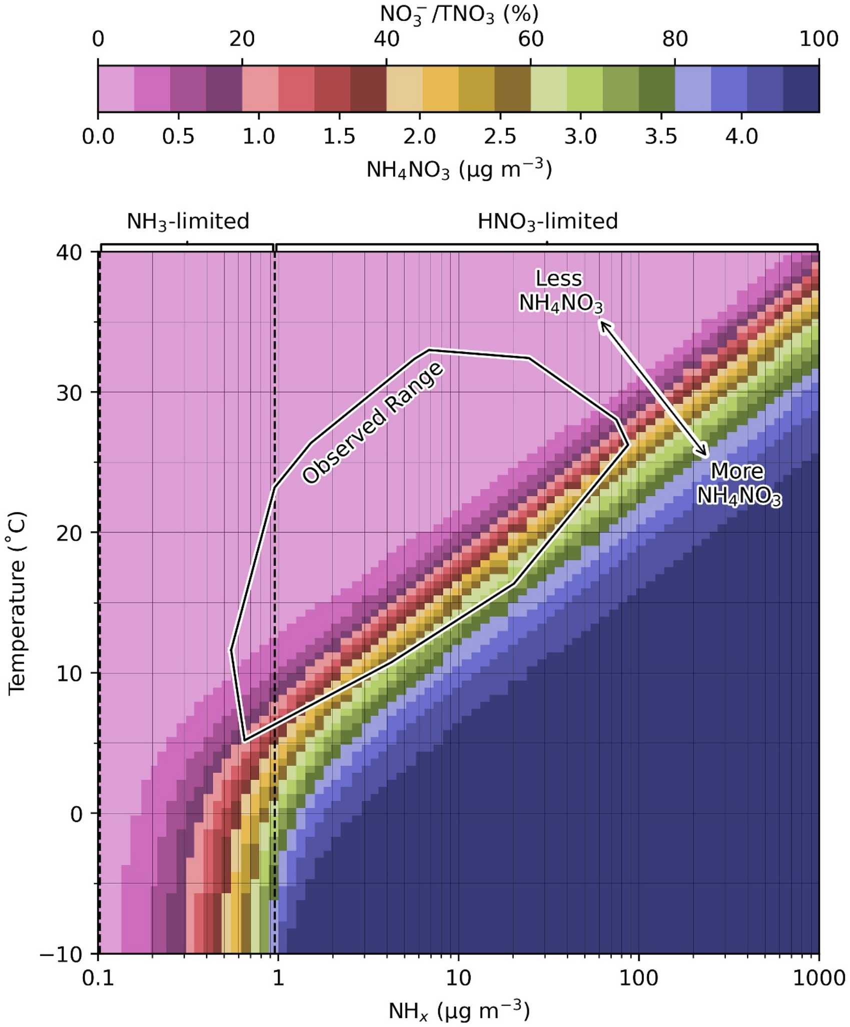

Figure 7. Modeled NH_4NO_3 and total nitrate partitioning (colorbar) for a sulfate-nitrate-ammonium system with fixed total nitrate, total sulfate, and RH for a range of temperatures and total ammonia concentrations. RH is set to dry conditions and TNO_3 is set to median observed total nitrate. The black outline shows the observed range of temperatures and NH_x during TRANS^{2}Am. NH_4NO_3 formation regimes are labeled on the top *x*-axis and delineated by the vertical black dashed lines.

characterized by regimes where NH_4NO_3 formation and partitioning to the aerosol phase is either (a) inhibited by warm temperatures and/or low NH_x (light pink region) or (b) very sensitive to both temperature and NH_x (steep NO_3^-/TNO_3 gradient in red, yellow, and green areas). The majority of observations fall in the first category, with 70% (448/642) in the <5% modeled NO_3^-/TNO_3 region and 92% (589/642) in the modeled $NO_3^-/TNO_3 < 20\%$ region. In the HNO_3-limited regime of Figure 7 at $NH_x \geq 0.9$ µg m^{-3} (gas ratio > 1), NH_4NO_3 formation is still very sensitive to temperature and NH_3, indicating a transition regime between when NH_4NO_3 formation is solely sensitive to NH_3 and HNO_3. In this transition regime, at the same NH_x concentration, a temperature difference of 1°C can result in a difference in NO_3^-/TNO_3 of as high as 12% (0.53 µg m^{-3} NH_4NO_3). Whereas Figure 7 shows model results from a simplified aerosol system, NH_3-HNO_3-NH_4NO_3 partitioning in the ambient atmosphere is affected by complex, non-linear relationships between temperature, RH (for aqueous aerosols), and concentrations of TNO_3, SO_4^{2-}, and other non-/semivolatile inorganic and organic compounds. We conduct sensitivity tests for various HNO_3 concentrations and RH observed during TRANS^{2}Am and find that the NH_4NO_3 mass concentration increases at a fixed NH_x concentration and temperature when TNO_3 increases, but the NO_3^- fraction of TNO_3 as a function of temperature and NH_x remains similar (Figure S12 in Supporting

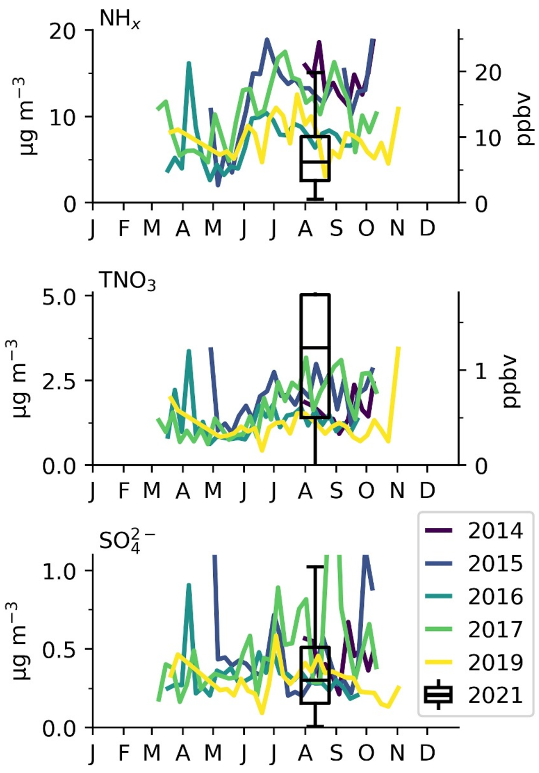

Figure 8. Weekly URG denuder/filter pack measurements of NH_x (top), TNO_3 (middle), and sulfate (bottom) in µg m^{-3} (left y-axis) and ppbv (right y-axis) at ambient temperature and pressure for March–October 2014–2017 and 2019 at the Weld County Tower surface monitoring site (40.386°N, 104.737°W) in Greeley, Colorado colored by year. Boxplot of TRANS^{2}Am Phase I measurements in 2021 are in black. Tails represent 1.5*IQR and extend from −0.9 to 8.7 µg m^{-3} for TNO_3.

Information S1), and the majority observations still fall within the <20% modeled NO_3^-/TNO_3 region (Table S2 in Supporting Information S1).

NH_4NO_3 formation can be sensitive to NH_3 in summertime AFO outflow even though it is largely HNO_3-limited. Figure S13 in Supporting Information S1 shows the change in modeled NH_4^+ and NO_3^- for simulations where NH_x and TNO_3 were respectively set to half of their measured concentrations. When NH_x is halved, modeled NH_4^+ and NO_3^- decrease in locations that are NH_3-limited. However, there are air masses sampled in the HNO_3-limited regime where NH_4^+ and NO_3^- also decrease. Similarly, when TNO_3 is halved, modeled NH_4^+ and NO_3^- consistently decrease in air masses in the HNO_3-limited regime; a decrease is also predicted for some NH_3-limited locations. This implies that many air masses are sensitive to both NH_3 and HNO_3, and reducing NH_3 emissions may still be effective in reducing NH_4NO_3 concentrations.

Temperature appears to be a strong driver of inorganic gas-aerosol partitioning, so accurate measurements are critical. We showed in Figure 7 that temperature differences as small as 1°C can result in a difference in a modeled NO_3^-/TNO_3 as large as 12%. Temperature measurements could be complicated by measurement errors or the aircraft cabin temperature within the research aircraft being warmer than the surrounding atmosphere, leading to NH_4^+ evaporation in the PILS inlet line and an overprediction in model NH_4^+. We are unable to directly compare cabin-ambient temperature gradients to model error because internal cabin temperature was not measured. Instead, we estimate NH_4NO_3 evaporation in the aerosol inlet line based on kinetic mass transfer equations from Dahneke (1983) and NH_4NO_3 equilibrium constants from Stelson and Seinfeld (1982) and find that the residence time in the aerosol inlet (2 s) is too short for significant NH_4^+ evaporation to occur (Section S2 in Supporting Information S1). Thus, a cabin-ambient temperature gradient may not be driving model-observation disagreement, but temperature differences on longer timescales may still have profound impacts on NH_4NO_3 formation.

3.5. Modeling the Seasonality of NH_4NO_3 Formation

Figure 8 shows the distribution of NH_x, TNO_3, and SO_4^{2-} measured during Phase I of TRANS^{2}Am relative to the weekly measurements of NH_x, TNO_3, and SO_4^{2-} from mid-March to mid-October in 2014–2019 (excluding 2018) at the Weld County Tower surface monitoring site in Greeley, Colorado. Greeley is an urban (population = 110,000) area within the study region and immediately surrounded by a large number of AFOs (Figure 1). These long-term surface-based measurements indicate no strong seasonality in NH_x, TNO_3, and SO_4^{2-} concentrations in close proximity to AFOs and urban traffic emissions.

2-min averaged NH_x concentrations observed during TRANS^{2}Am are lower than long-term observations, and there are several potential reasons why we might expect this: (a) NH_x is dominated by NH_3, and $NH_3$was measured aloft (300–1,500 m agl) during TRANS^{2}Am. Away from individual facilities, NH_3 typically maximizes at 10 m agl (Y. Li et al., 2017), and (b) the aircraft has sampled a much larger region and range of altitudes than represented by the ground observations.

TNO_3 measured during TRANS^{2}Am is higher than the ground-based measurements, which may be because (a) the diurnal cycle of HNO_3 and (b) the influence from wildfire smoke. During summertime, active photochemistry drives a peak in HNO_3 between 11 a.m. and 2 p.m. local time Lindaas et al. (2017). Thus, most of the TRANS^{2}Am flights were conducted when HNO_3 concentrations are largest. Summer 2021 was also an active wildfire season, and HNO_3 is the second highest constituent of NO_y in aged wildfire smoke at low altitudes (Juncosa Calahorrano et al., 2021).

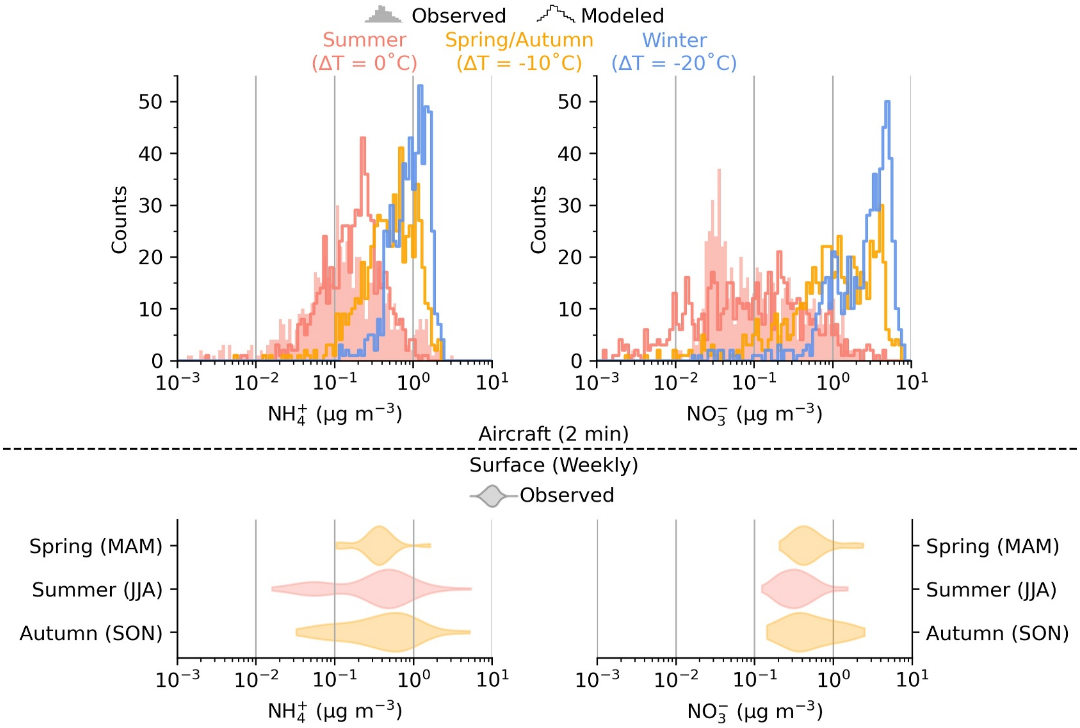

Figure 9. Seasonality of observed (shades) and modeled (lines) NH_4^+ (left) and NO_3^- (right). Top: histograms of observed and modeled NH_4^+ and NO_3^- along the flight track. Red shade is observations during summer, red line is model with observed temperature during summer ($\Delta T = 0$°C), yellow line is model with observed temperature minus 10°C ($\Delta T = -10$°C) to simulate spring/fall, and blue line is model with observed temperature minus 20°C ($\Delta T = -20$°C) to simulate winter. Bottom: violin plots of weekly surface-based NH_4^+ and NO_3^- observed at the Weld County Tower site in Greeley, Colorado grouped by meteorological season. Note no observations made during winter (DJF).

Finally, sulfate concentrations are consistent between TRANS^{2}Am and the long–term measurements at Weld County Tower, and do not exhibit a strong seasonality. This is consistent with Chan et al. (2018), who observed no sulfate seasonality across the US after 2008. Since neither NH_x, TNO_3, nor SO_4^{2-} show a strong seasonal pattern, we model the seasonality of NH_4NO_3 formation by varying only temperature.

We investigate the seasonality of NH_4NO_3 formation for average temperature conditions in northeastern Colorado using E-AIM and hypothesize the existence of significantly higher concentrations in spring/autumn and winter due to the strong sensitivity to temperature. We model spring/autumn by lowering the model temperature by 10°C relative to campaign observations during the summer, and winter conditions by lowering the temperature by 20°C to capture the seasonal temperature ranges in this study region.

Figure 9 shows consistently more NH_4^+ and NO_3^- during these cooler seasons, indicating NH_4NO_3 formation is thermodynamically favorable significantly more often in spring/autumn and winter. Instances of significant NH_4NO_3 formation >1, >3, and >5 μg m^{-3} are summarized in Table 2, and $NH_4NO_3 > 1$ μg m^{-3} is almost 10 times more likely in the winter than in the summer. In August 2021, no $NH_4NO_3 > 3$ μg m^{-3} was observed and

Table 2
Percent of Time That NH_4NO_3 Is Greater Than Thresholds of 1, 3, and 5 μg m^{-3} for the Observations, Model Output Along the Flight Tracks, and the Model Simulations Where the Temperature Was Reduced by 10 and 20°C

	Observed	Modeled		
	Summer	Summer ($\Delta T = 0$°C)	Spring/Autumn ($\Delta T = -10$°C)	Winter ($\Delta T = -20$°C)
$NH_4NO_3 \geq 1$ μg m^{-3}	10% (61/634)	9% (56/612)	61% (375/612)	88% (537/612)
$NH_4NO_3 \geq 3$ μg m^{-3}	0% (0/634)	2% (10/612)	28% (171/612)	60% (365/612)
$NH_4NO_3 \geq 5$ μg m^{-3}	0% (0/634)	0.3% (2/612)	11% (69/612)	35% (213/612)

very little was modeled, but the model suggests that significantly more is likely present in spring/autumn and winter. These modeling results imply that even though NH_4NO_3 formation is HNO_3-limited and generally inhibited by hot temperatures during TRANS^{2}Am, high concentrations of NH_3 (>5 ppbv) could contribute to significant $PM_{2.5}$ formation under cooler conditions given the weak seasonal cycle in precursors (Figure 8). The distributions of modeled NH_4^+ and NO_3^- along the flight track generally captures the range of surface observations by season, but best represent diurnal maximum NH_3 and HNO_3 emissions as opposed to the weekly-integrated surface measurements.

We evaluated whether we expect NH_3 plumes from AFOs to enhance NH_4NO_3 concentrations relative to background during cooler seasons (Figure S16 in Supporting Information S1). Summertime and wintertime NH_4NO_3 formation in and out of plumes is more sensitive to the temperature differences between seasons than the differences in NH_3 in and out of a plume, whereas NH_4NO_3 formation in spring/autumn is sensitive to both temperature and the NH_3 changes (Figure S16 in Supporting Information S1). In the summer, both the model and observations agree NH_4NO_3 is typically <1 μg m^{-3} both in the background ($NH_3 < 20$ ppbv) and in plumes ($NH_3 \geq 20$ ppbv) and inhibited by warm temperatures. In the winter, the median NH_4NO_3 increases from 2.8 μg m^{-3} in the background to 4.6 μg m^{-3} in plumes. In spring/autumn, the median NH_4NO_3 is still relatively low (0.9 μg m^{-3}) in the background but increases to 3.6 μg m^{-3} in plumes. These results suggest a transition from summertime temperature-inhibited NH_4NO_3 formation to wintertime temperature-saturated NH_4NO_3 formation and an intermediate temperature- and NH_3-sensitive regime in the transitional seasons.

4. Conclusions

In this work, we present the application of the E-AIM aerosol thermodynamic model to agricultural plumes from AFOs under hot, dry summertime conditions in Northern Colorado. With a holistic data set of aircaft-based gas-phase and aerosol-phase measurements from Phase I of the TRANS^{2}Am campaign, we (a) study the sensitivity of NH_4NO_3 formation to summertime AFO emissions of NH_3 and (b) predict the seasonality of NH_4NO_3 formation in northeastern Colorado. We find that:

- Summertime northeastern Colorado is NH_3-rich and HNO_3-limited.
- During August 2021, the observed range of NH_3-NH_4^+ and HNO_3-NO_3^- partitioning on aggregate can generally be explained by the E-AIM aerosol thermodynamic model with temperature, relative humidity, NH_x ($NH_3 + NH_4^+$), TNO_3 ($HNO_3 + NO_3^-$), SO_4^{2-}, oxalate, formate, and acetate as inputs.
- The airborne observed summertime NH_4NO_3 concentration is usually <1 μg m^{-3} above 300 m agl and its formation is thermodynamically inhibited by hot temperatures.
- The NH_4NO_3 formation observed during Phase I of TRANS^{2}Am is especially sensitive to temperature and NH_x. The campaign sampled a wide range of NH_3 concentrations (0.5–114 ppbv, 2 min averages) and temperatures between 5 and 33°C. Model sensitivity tests suggest that a small change in temperature of 1°C under these NH_3 concentrations can change NH_4NO_3 formation by as much as 12%.
- We use E-AIM to predict that NH_4NO_3 could reach substantial (>1 μg m^{-3}) concentrations spring/autumn and winter in northeastern Colorado due to cooler temperatures.

We demonstrate that with a comprehensive data set of high temporal resolution aircraft-based gas-phase and aerosol-phase measurements, aerosol thermodynamic models can be leveraged to study the inorganic gas-aerosol partitioning of the NH_3-HNO_3-NH_4NO_3 system from large NH_3 point sources. Thus, similar payloads that measure both NH_3 and HNO_3 gases and aerosols at high sub-hour resolutions can then also be used to study NH_3-NH_4^+ partitioning in agricultural regions. Future work should include similar measurements made under a wider range of conditions, particularly under cooler conditions.

Data Availability Statement

The TRANS^{2}Am data used in this manuscript is publicly available on the NCAR/UCAR EOL Data Archive (https://data.eol.ucar.edu/dataset/list?project=606&children=project, Caulton & McCabe, 2022; French et al., 2023; Sullivan & Fischer, 2023). The weekly ground-based measurements from Greeley, Colorado is publicly available on Zenodo (https://doi.org/10.5281/zenodo.10855259, Sullivan, 2024). The E-AIM model input and output data is publicly accessible on Zenodo (https://doi.org/10.5281/zenodo.10855157, E. Li, 2024).

Acknowledgments

We would like to thank the University of Wyoming King Air team for their support in data collection, Evelyn Bangs for her help in preparing and collecting the URG samples in Greeley, Colorado, and Allie Mazurek and Marqi Rocque for providing daily forecasting during phase I of TRANS^{2}Am. We would also like to thank two anonymous reviewers for their feedback to improve this work. This work was supported by the National Science Foundation (NSF, Award 2020127 and 2020151) and the National Oceanic and Atmospheric Administration (NOAA, Award NA21OAR4310128).

References

Ansari, A. S., & Pandis, S. N. (1998). Response of inorganic PM to precursor concentrations. *Environmental Science & Technology*, *32*(18), 2706–2714. https://doi.org/10.1021/es971130j

Ayers, G. P., Gillett, R. W., & Gras, J. L. (1980). On the vapor pressure of sulfuric acid. *Geophysical Research Letters*, *7*(6), 433–436. https://doi.org/10.1029/GL007i006p00433

Bassett, M., & Seinfeld, J. H. (1983). Atmospheric equilibrium model of sulfate and nitrate aerosols. *Atmospheric Environment*, *17*(11), 2237–2252. https://doi.org/10.1016/0004-6981(83)90221-4

Behera, S. N., Sharma, M., Aneja, V. P., & Balasubramanian, R. (2013). Ammonia in the atmosphere: A review on emission sources, atmospheric chemistry and deposition on terrestrial bodies. *Environmental Science and Pollution Research*, *20*(11), 8092–8131. https://doi.org/10.1007/s11356-013-2051-9

Benedict, K. B., Chen, X., Sullivan, A. P., Li, Y., Day, D., Prenni, A. J., et al. (2013). Atmospheric concentrations and deposition of reactive nitrogen in Grand Teton National Park. *Journal of Geophysical Research: Atmospheres*, *118*(20), 11875–11887. https://doi.org/10.1002/2013JD020394

Benedict, K. B., Day, D., Schwandner, F. M., Kreidenweis, S. M., Schichtel, B., Malm, W. C., & Collett, J. L. (2013). Observations of atmospheric reactive nitrogen species in Rocky Mountain National Park and across northern Colorado. *Atmospheric Environment*, *64*, 66–76. https://doi.org/10.1016/j.atmosenv.2012.08.066

Benedict, K. B., Prenni, A. J., Sullivan, A. P., Evanoski-Cole, A. R., Fischer, E. V., Callahan, S., et al. (2018). Impact of Front range sources on reactive nitrogen concentrations and deposition in Rocky Mountain National Park. *PeerJ*, *6*, e4759. https://doi.org/10.7717/peerj.4759

Caulton, D., & McCabe, M. (2022). TRANS2AM: King air Picarro G2401-M 2021 phase data. Version 2.0 [Dataset]. *UCAR/NCAR – Earth Observing Laboratory*. https://doi.org/10.26023/8EMT-47X7-VV00

Chan, E. A. W., Gantt, B., & McDow, S. (2018). The reduction of summer sulfate and switch from summertime to wintertime $PM_{2.5}$ concentration maxima in the United States. *Atmospheric Environment*, *175*, 25–32. https://doi.org/10.1016/j.atmosenv.2017.11.055

Chen, D., Yao, X., Chan, C. K., Tian, X., Chu, Y., Clegg, S. L., et al. (2022). Competitive uptake of dimethylamine and trimethylamine against ammonia on acidic particles in marine atmospheres. *Environmental Science & Technology*, *56*(9), 5430–5439. https://doi.org/10.1021/acs.est.1c08713

Cheng, B., Wang-Li, L., Meskhidze, N., Classen, J., & Bloomfield, P. (2021). Partitioning of NH_3-NH_4^+ in the southeastern U.S. *Atmosphere*, *12*(12), 1681. https://doi.org/10.3390/atmos12121681

Choi, M. Y., & Chan, C. K. (2002). The effects of organic species on the hygroscopic behaviors of inorganic aerosols. *Environmental Science & Technology*, *36*(11), 2422–2428. https://doi.org/10.1021/es0113293

Clegg, S. L., Brimblecombe, P., & Wexler, A. S. (1998). Thermodynamic model of the system H^+–NH_4^+–SO_4^{2-}–NO_3^-–H_2O at tropospheric temperatures. *The Journal of Physical Chemistry A*, *102*(12), 2137–2154. https://doi.org/10.1021/jp973042r

Clegg, S. L., Seinfeld, J. H., & Brimblecombe, P. (2001). Thermodynamic modelling of aqueous aerosols containing electrolytes and dissolved organic compounds. *Journal of Aerosol Science*, *32*(6), 713–738. https://doi.org/10.1016/S0021-8502(00)00105-1

Dahneke, B. (1983). Simple kinetic theory of Brownian diffusion in vapors and aerosols. In R. E. Meyer (Ed.), *Theory of dispersed multiphase flow* (pp. 97–133). Academic Press. https://doi.org/10.1016/B978-0-12-493120-6.50011-8

Davis, R. D., Lance, S., Gordon, J. A., Ushijima, S. B., & Tolbert, M. A. (2015). Contact efflorescence as a pathway for crystallization of atmospherically relevant particles. *Proceedings of the National Academy of Sciences of the United States of America*, *112*(52), 15815–15820. https://doi.org/10.1073/pnas.1522860113

Day, D. E., Chen, X., Gebhart, K. A., Carrico, C. M., Schwandner, F. M., Benedict, K. B., et al. (2012). Spatial and temporal variability of ammonia and other inorganic aerosol species. *Atmospheric Environment*, *61*, 490–498. https://doi.org/10.1016/j.atmosenv.2012.06.045

Di Lorenzo, R. A., Place, B. K., VandenBoer, T. C., & Young, C. J. (2018). Composition of size-resolved aged boreal fire aerosols: Brown carbon, biomass burning tracers, and reduced nitrogen. *ACS Earth and Space Chemistry*, *2*(3), 278–285. https://doi.org/10.1021/acsearthspacechem.7b00137

Eilerman, S. J., Peischl, J., Neuman, J. A., Ryerson, T. B., Aikin, K. C., Holloway, M. W., et al. (2016). Characterization of ammonia, methane, and nitrous oxide emissions from concentrated animal feeding operations in northeastern Colorado. *Environmental Science & Technology*, *50*(20), 10885–10893. https://doi.org/10.1021/acs.est.6b02851

Ellis, R. A., Murphy, J. G., Pattey, E., van Haarlem, R., O'Brien, J. M., & Herndon, S. C. (2010). Characterizing a quantum cascade tunable infrared laser differential absorption spectrometer (QC-TILDAS) for measurements of atmospheric ammonia. *Atmospheric Measurement Techniques*, *3*(2), 397–406. https://doi.org/10.5194/amt-3-397-2010

Erisman, J. W., Sutton, M. A., Galloway, J., Klimont, Z., & Winiwarter, W. (2008). How a century of ammonia synthesis changed the world. *Nature Geoscience*, *1*(10), 636–639. https://doi.org/10.1038/ngeo325

Evangeliou, N., Balkanski, Y., Eckhardt, S., Cozic, A., Van Damme, M., Coheur, P.-F., et al. (2021). 10-year satellite-constrained fluxes of ammonia improve performance of chemistry transport models. *Atmospheric Chemistry and Physics*, *21*(6), 4431–4451. https://doi.org/10.5194/acp-21-4431-2021

Fang, Z., Dong, S., Huang, C., Jia, S., Wang, F., Liu, H., et al. (2023). On using an aerosol thermodynamic model to calculate aerosol acidity of coarse particles. *Journal of Environmental Sciences*, *148*, 46–56. https://doi.org/10.1016/j.jes.2023.07.001

Fountoukis, C., & Nenes, A. (2007). ISORROPIA II: A computationally efficient thermodynamic equilibrium model for K^+–Ca^{2+}–Mg^{2+}–NH_4^+–Na^+–SO_4^{2-}–NO_3^-–Cl^-–H_2O aerosols. *Atmospheric Chemistry and Physics*, *7*(17), 4639–4659. https://doi.org/10.5194/acp-7-4639-2007

Franchin, A., Fibiger, D. L., Goldberger, L., McDuffie, E. E., Moravek, A., Womack, C. C., et al. (2018). Airborne and ground-based observations of ammonium-nitrate-dominated aerosols in a shallow boundary layer during intense winter pollution episodes in northern Utah. *Atmospheric Chemistry and Physics*, *18*(23), 17259–17276. https://doi.org/10.5194/acp-18-17259-2018

French, J., Oolman, L., & Plummer, D. (2023). University of Wyoming king air (UWKA) high-rate flight level data for TRANS2AM 2021 phase version 1.0 [Dataset]. *UCAR/NCAR - Earth Observing Laboratory*. https://doi.org/10.26023/TKV3-WJ7T-PP0J

Friese, E., & Ebel, A. (2010). Temperature dependent thermodynamic model of the system H^+–NH_4^+–Na^+–SO_4^{2-}–NO_3^-–Cl^-–H_2O. *The Journal of Physical Chemistry A*, *114*(43), 11595–11631. https://doi.org/10.1021/jp101041j

Galloway, J. N., Dentener, F. J., Capone, D. G., Boyer, E. W., Howarth, R. W., Seitzinger, S. P., et al. (2004). Nitrogen cycles: Past, present, and future. *Biogeochemistry*, *70*(2), 153–226. https://doi.org/10.1007/s10533-004-0370-0

Guo, H., Otjes, R., Schlag, P., Kiendler-Scharr, A., Nenes, A., & Weber, R. J. (2018). Effectiveness of ammonia reduction on control of fine particle nitrate. *Atmospheric Chemistry and Physics*, *18*(16), 12241–12256. https://doi.org/10.5194/acp-18-12241-2018

Guo, H., Sullivan, A. P., Campuzano-Jost, P., Schroder, J. C., Lopez-Hilfiker, F. D., Dibb, J. E., et al. (2016). Fine particle pH and the partitioning of nitric acid during winter in the northeastern United States. *Journal of Geophysical Research: Atmospheres*, *121*(17), 10355–10376. https://doi.org/10.1002/2016JD025311

Hacker, J. M., Chen, D., Bai, M., Ewenz, C., Junkermann, W., Lieff, W., et al. (2016). Using airborne technology to quantify and apportion emissions of CH_4 and NH_3 from feedlots. *Animal Production Science*, *56*(3), 190–203. https://doi.org/10.1071/AN15513

Hand, J. L., Prenni, A. J., Copeland, S., Schichtel, B. A., & Malm, W. C. (2020). Thirty years of the clean air act amendments: Impacts on haze in remote regions of the United States (1990–2018). *Atmospheric Environment*, *243*, 117865. https://doi.org/10.1016/j.atmosenv.2020.117865

Hennigan, C. J., Izumi, J., Sullivan, A. P., Weber, R. J., & Nenes, A. (2015). A critical evaluation of proxy methods used to estimate the acidity of atmospheric particles. *Atmospheric Chemistry and Physics*, *15*(5), 2775–2790. https://doi.org/10.5194/acp-15-2775-2015

Hristov, A. N., Hanigan, M., Cole, A., Todd, R., McAllister, T. A., Ndegwa, P. M., & Rotz, A. (2011). Review: Ammonia emissions from dairy farms and beef feedlots. *Canadian Journal of Animal Science*, *91*(1), 1–35. https://doi.org/10.4141/CJAS10034

Jimenez, J. L., Canagaratna, M. R., Donahue, N. M., Prevot, A. S. H., Zhang, Q., Kroll, J. H., et al. (2009). Evolution of organic aerosols in the atmosphere. *Science*, *326*(5959), 1525–1529. https://doi.org/10.1126/science.1180353

Juncosa Calahorrano, J. F., Lindaas, J., O'Dell, K., Palm, B. B., Peng, Q., Flocke, F., et al. (2021). Daytime oxidized reactive nitrogen partitioning in western U.S. wildfire smoke plumes. *Journal of Geophysical Research: Atmospheres*, *126*(4), e2020JD033484. https://doi.org/10.1029/2020JD033484

Juncosa Calahorrano, J. F., Pollack, I. B., Sullivan, A. P., Roscioli, J. R., Caulton, D. R., McCabe, M. E., et al. (2023). Summertime airborne measurements of ammonia emissions from cattle feedlots and dairies in northeastern Colorado. *Journal of Geophysical Research: Atmospheres*, *128*(23), e2023JD039043. https://doi.org/10.1029/2023JD039043

Kim, Y. P., Seinfeld, J. H., & Saxena, P. (1993). Atmospheric gas-aerosol equilibrium I. Thermodynamic model. *Aerosol Science and Technology*, *19*(2), 157–181. https://doi.org/10.1080/02786829308959628

Kulmala, M., & Laaksonen, A. (1990). Binary nucleation of water–sulfuric acid system: Comparison of classical theories with different H_2SO_4 saturation vapor pressures. *The Journal of Chemical Physics*, *93*(1), 696–701. https://doi.org/10.1063/1.459519

Lawrence, C. E., Casson, P., Brandt, R., Schwab, J. J., Dukett, J. E., Snyder, P., et al. (2023). Long-term monitoring of cloud water chemistry at whiteface mountain: The emergence of a new chemical regime. *Atmospheric Chemistry and Physics*, *23*(2), 1619–1639. https://doi.org/10.5194/acp-23-1619-2023

Li, E. (2024). TRANS^{2}Am phase I EAIM model data [Dataset]. *Zenodo*. https://doi.org/10.5281/zenodo.10855157

Li, Y., Thompson, T. M., Van Damme, M., Chen, X., Benedict, K. B., Shao, Y., et al. (2017). Temporal and spatial variability of ammonia in urban and agricultural regions of northern Colorado, United States. *Atmospheric Chemistry and Physics*, *17*(10), 6197–6213. https://doi.org/10.5194/acp-17-6197-2017

Liggio, J., Li, S.-M., Vlasenko, A., Stroud, C., & Makar, P. (2011). Depression of ammonia uptake to sulfuric acid aerosols by competing uptake of ambient organic gases. *Environmental Science & Technology*, *45*(7), 2790–2796. https://doi.org/10.1021/es103801g

Lindaas, J., Farmer, D. K., Pollack, I. B., Abeleira, A., Flocke, F., Roscioli, R., et al. (2017). Changes in ozone and precursors during two aged wildfire smoke events in the Colorado front range in summer 2015. *Atmospheric Chemistry and Physics*, *17*(17), 10691–10707. https://doi.org/10.5194/acp-17-10691-2017

Liu, L., Xu, W., Lu, X., Zhong, B., Guo, Y., Lu, X., et al. (2022). Exploring global changes in agricultural ammonia emissions and their contribution to nitrogen deposition since 1980. *Proceedings of the National Academy of Sciences of the United States of America*, *119*(14), e2121998119. https://doi.org/10.1073/pnas.2121998119

Luo, Z., Zhang, Y., Chen, W., Van Damme, M., Coheur, P.-F., & Clarisse, L. (2022). Estimating global ammonia (NH_3) emissions based on IASI observations from 2008 to 2018. *Atmospheric Chemistry and Physics*, *22*(15), 10375–10388. https://doi.org/10.5194/acp-22-10375-2022

Marple, V. A., Rubow, K. L., & Behm, S. M. (1991). A microorifice uniform deposit impactor (MOUDI): Description, calibration, and use. *Aerosol Science and Technology*, *14*(4), 434–446. https://doi.org/10.1080/02786829108959504

McCabe, M. E., Pollack, I. B., Fischer, E. V., Steinmann, K. M., & Caulton, D. R. (2023). Technical note: Isolating methane emissions from animal feeding operations in an interfering location. *Atmospheric Chemistry and Physics*, *23*(13), 7479–7494. https://doi.org/10.5194/acp-23-7479-2023

McManus, J. B., Kebabian, P. L., & Zahniser, M. S. (1995). Astigmatic mirror multipass absorption cells for long-path-length spectroscopy. *Applied Optics*, *34*(18), 3336–3348. https://doi.org/10.1364/AO.34.003336

McManus, J. B., Zahniser, M. S., Jr, D. D. N., Shorter, J. H., Herndon, S. C., Wood, E. C., & Wehr, R. (2010). Application of quantum cascade lasers to high-precision atmospheric trace gas measurements. *Optical Engineering*, *49*(11), 111124. https://doi.org/10.1117/1.3498782

Meng, Z., & Seinfeld, J. H. (1996). Time scales to achieve atmospheric gas-aerosol equilibrium for volatile species. *Atmospheric Environment*, *30*(16), 2889–2900. https://doi.org/10.1016/1352-2310(95)00493-9

Metzger, S., Mihalopoulos, N., & Lelieveld, J. (2006). Importance of mineral cations and organics in gas-aerosol partitioning of reactive nitrogen compounds: Case study based on MINOS results. *Atmospheric Chemistry and Physics*, *6*(9), 2549–2567. https://doi.org/10.5194/acp-6-2549-2006

Miller, D. J., Sun, K., Tao, L., Pan, D., Zondlo, M. A., Nowak, J. B., et al. (2015). Ammonia and methane dairy emission plumes in the San Joaquin Valley of California from individual feedlot to regional scales. *Journal of Geophysical Research: Atmospheres*, *120*(18), 9718–9738. https://doi.org/10.1002/2015JD023241

Murphy, J. G., Gregoire, P. K., Tevlin, A. G., Wentworth, G. R., Ellis, R. A., Markovic, M. Z., & VandenBoer, T. C. (2017). Observational constraints on particle acidity using measurements and modelling of particles and gases. *Faraday Discussions*, *200*, 379–395. https://doi.org/10.1039/C7FD00086C

Nah, T., Guo, H., Sullivan, A. P., Chen, Y., Tanner, D. J., Nenes, A., et al. (2018). Characterization of aerosol composition, aerosol acidity, and organic acid partitioning at an agriculturally intensive rural southeastern US site. *Atmospheric Chemistry and Physics*, *18*(15), 11471–11491. https://doi.org/10.5194/acp-18-11471-2018

Nair, A. A., & Yu, F. (2020). Quantification of atmospheric ammonia concentrations: A review of its measurement and modeling. *Atmosphere*, *11*(10), 1092. https://doi.org/10.3390/atmos11101092

NEI (National Emissions Inventory). (2020). *NEI (National Emissions Inventory)*. United States Environmental Protection Agency. Retrieved from https://www.epa.gov/air-emissions-inventories/2020-national-emissions-inventory-nei-data

Neuman, J. A., Ryerson, T. B., Huey, L. G., Jakoubek, R., Nowak, J. B., Simons, C., & Fehsenfeld, F. C. (2003). Calibration and evaluation of nitric acid and ammonia permeation tubes by UV optical absorption. *Environmental Science & Technology*, *37*(13), 2975–2981. https://doi.org/10.1021/es026422l

Nowak, J. B., Neuman, J. A., Bahreini, R., Brock, C. A., Middlebrook, A. M., Wollny, A. G., et al. (2010). Airborne observations of ammonia and ammonium nitrate formation over Houston, Texas. *Journal of Geophysical Research*, *115*(D22), D22304. https://doi.org/10.1029/2010JD014195

Nowak, J. B., Neuman, J. A., Bahreini, R., Middlebrook, A. M., Holloway, J. S., McKeen, S. A., et al. (2012). Ammonia sources in the California South Coast Air Basin and their impact on ammonium nitrate formation. *Geophysical Research Letters*, *39*(7), L07804. https://doi.org/10.1029/2012GL051197

Orsini, D. A., Ma, Y., Sullivan, A. P., Sierau, B., Baumann, K., & Weber, R. J. (2003). Refinements to the particle-into-liquid sampler (PILS) for ground and airborne measurements of water soluble aerosol composition. *Atmospheric Environment*, *37*(9), 1243–1259. https://doi.org/10.1016/S1352-2310(02)01015-4

Pan, D., Benedict, K. B., Golston, L. M., Wang, R., Collett, J. L., Tao, L., et al. (2021). Ammonia dry deposition in an alpine ecosystem traced to agricultural emission hotpots. *Environmental Science & Technology*, *55*(12), 7776–7785. https://doi.org/10.1021/acs.est.0c05749

Pant, A., Fok, A., Parsons, M. T., Mak, J., & Bertram, A. K. (2004). Deliquescence and crystallization of ammonium sulfate-glutaric acid and sodium chloride-glutaric acid particles. *Geophysical Research Letters*, *31*(12), L12111. https://doi.org/10.1029/2004GL020025

Permar, W., Wielgasz, C., Jin, L., Chen, X., Coggon, M. M., Garofalo, L. A., et al. (2023). Assessing formic and acetic acid emissions and chemistry in western U.S. Wildfire smoke: Implications for atmospheric modeling. *: Atmospheres*, *3*(11), 1620–1641. https://doi.org/10.1039/D3EA00098B

Petters, M. D., & Kreidenweis, S. M. (2007). A single parameter representation of hygroscopic growth and cloud condensation nucleus activity. *Atmospheric Chemistry and Physics*, *7*(8), 1961–1971. https://doi.org/10.5194/acp-7-1961-2007

Pollack, I. B., Lindaas, J., Roscioli, J. R., Agnese, M., Permar, W., Hu, L., & Fischer, E. V. (2019). Evaluation of ambient ammonia measurements from a research aircraft using a closed-path QC-TILDAS operated with active continuous passivation. *Atmospheric Measurement Techniques*, *12*(7), 3717–3742. https://doi.org/10.5194/amt-12-3717-2019

Pollack, I. B., McCabe, M. E., Caulton, D. R., & Fischer, E. V. (2022). Enhancements in ammonia and methane from agricultural sources in the northeastern Colorado front range using observations from a small research aircraft. *Environmental Science & Technology*, *56*(4), 2236–2247. https://doi.org/10.1021/acs.est.1c07382

Pope, C. A., Ezzati, M., & Dockery, D. W. (2009). Fine-particulate air pollution and life expectancy in the United States. *New England Journal of Medicine*, *360*(4), 376–386. https://doi.org/10.1056/NEJMsa0805646

Pun, B. K., Griffin, R. J., Seigneur, C., & Seinfeld, J. H. (2002). Secondary organic aerosol 2. Thermodynamic model for gas/particle partitioning of molecular constituents. *Journal of Geophysical Research*, *107*(D17), AAC4-1–AAC4-15. https://doi.org/10.1029/2001JD000542

Pye, H. O. T., Nenes, A., Alexander, B., Ault, A. P., Barth, M. C., Clegg, S. L., et al. (2020). The acidity of atmospheric particles and clouds. *Atmospheric Chemistry and Physics*, *20*(8), 4809–4888. https://doi.org/10.5194/acp-20-4809-2020

Riemer, N., Ault, A. P., West, M., Craig, R. L., & Curtis, J. H. (2019). Aerosol mixing state: Measurements, modeling, and impacts. *Reviews of Geophysics*, *57*(2), 187–249. https://doi.org/10.1029/2018RG000615

Robarge, W. P., Walker, J. T., McCulloch, R. B., & Murray, G. (2002). Atmospheric concentrations of ammonia and ammonium at an agricultural site in the southeast United States. *Atmospheric Environment*, *36*(10), 1661–1674. https://doi.org/10.1016/S1352-2310(02)00171-1

Roedel, W. (1979). Measurement of sulfuric acid saturation vapor pressure; Implications for aerosol formation by heteromolecular nucleation. *Journal of Aerosol Science*, *10*(4), 375–386. https://doi.org/10.1016/0021-8502(79)90032-6

Rood, M. J., Shaw, M. A., Larson, T. V., & Covert, D. S. (1989). Ubiquitous nature of ambient metastable aerosol. *Nature*, *337*(6207), 537–539. https://doi.org/10.1038/337537a0

Roscioli, J. R., Zahniser, M. S., Nelson, D. D., Herndon, S. C., & Kolb, C. E. (2016). New approaches to measuring sticky molecules: Improvement of instrumental response times using active passivation. *The Journal of Physical Chemistry A*, *120*(9), 1347–1357. https://doi.org/10.1021/acs.jpca.5b04395

Russell, A. G., McRae, G. J., & Cass, G. R. (1983). Mathematical modeling of the formation and transport of ammonium nitrate aerosol. *Atmospheric Environment*, *17*(5), 949–964. https://doi.org/10.1016/0004-6981(83)90247-0

Sander, R. (2023). Compilation of Henry's law constants (version 5.0.0) for water as solvent. *Atmospheric Chemistry and Physics*, *23*(19), 10901–12440. https://doi.org/10.5194/acp-23-10901-2023

Schlag, P., Rubach, F., Mentel, T. F., Reimer, D., Canonaco, F., Henzing, J. S., et al. (2017). Ambient and laboratory observations of organic ammonium salts in PM1. *Faraday Discussions*, *200*(0), 331–351. https://doi.org/10.1039/C7FD00027H

Schobesberger, S., D'Ambro, E. L., Vettikkat, L., Lee, B. H., Peng, Q., Bell, D. M., et al. (2023). Airborne flux measurements of ammonia over the southern Great Plains using chemical ionization mass spectrometry. *Atmospheric Measurement Techniques*, *16*(2), 247–271. https://doi.org/10.5194/amt-16-247-2023

Snider, J., Petters, M., Takagi, H., Liu, P., Lukens, D., Glover, B., et al. (2018). *The NCAR-UWyo aerosol inlet*. The University of Wyoming. Retrieved from http://www-das.uwyo.edu/~jsnider/inlet_report_v02.pdf

Song, S., Gao, M., Xu, W., Shao, J., Shi, G., Wang, S., et al. (2018). Fine-particle pH for Beijing winter haze as inferred from different thermodynamic equilibrium models. *Atmospheric Chemistry and Physics*, *18*(10), 7423–7438. https://doi.org/10.5194/acp-18-7423-2018

Sorooshian, A., Brechtel, F. J., Ma, Y., Weber, R. J., Corless, A., Flagan, R. C., & Seinfeld, J. H. (2006). Modeling and characterization of a particle-into-liquid sampler (PILS). *Aerosol Science and Technology*, *40*(6), 396–409. https://doi.org/10.1080/02786820600632282

Sorooshian, A., Murphy, S. M., Hersey, S., Gates, H., Padro, L. T., Nenes, A., et al. (2008). Comprehensive airborne characterization of aerosol from a major bovine source. *Atmospheric Chemistry and Physics*, *8*(17), 5489–5520. https://doi.org/10.5194/acp-8-5489-2008

Staebler, R. M., McGinn, S. M., Crenna, B. P., Flesch, T. K., Hayden, K. L., & Li, S.-M. (2009). Three-dimensional characterization of the ammonia plume from a beef cattle feedlot. *Atmospheric Environment*, *43*(38), 6091–6099. https://doi.org/10.1016/j.atmosenv.2009.08.045

Stelson, A. W., Friedlander, S. K., & Seinfeld, J. H. (1979). A note on the equilibrium relationship between ammonia and nitric acid and particulate ammonium nitrate. *Atmospheric Environment*, *13*(3), 369–371. https://doi.org/10.1016/0004-6981(79)90293-2

Stelson, A. W., & Seinfeld, J. H. (1982). Relative humidity and temperature dependence of the ammonium nitrate dissociation constant. *Atmospheric Environment*, *16*(5), 983–992. https://doi.org/10.1016/0004-6981(82)90184-6

Sullivan, A. P. (2024). Weekly ground-based measurements of NH_3, HNO_3, and submicron aerosol composition from Greeley, Colorado [Dataset]. *Zenodo*. https://doi.org/10.5281/zenodo.10855259

Sullivan, A. P., & Fischer, E. (2023). TRANS2AM: King air PILS water-soluble aerosol components data version 2.0 [Dataset]. *UCAR/NCAR – Earth Observing Laboratory*. https://doi.org/10.26023/680R-9WEZ-N70H

Sullivan, A. P., Frank, N., Kenski, D. M., & Collett, J. L., Jr. (2011). Application of high-performance anion-exchange chromatography–pulsed amperometric detection for measuring carbohydrates in routine daily filter samples collected by a national network: 2. Examination of sugar alcohols/polyols, sugars, and anhydrosugars in the upper midwest. *Journal of Geophysical Research*, *116*(D8), D08303. https://doi.org/10.1029/2010JD014169

Sullivan, A. P., Frank, N., Onstad, G., Simpson, C. D., & Collett, J. L., Jr. (2011). Application of high-performance anion-exchange chromatography–pulsed amperometric detection for measuring carbohydrates in routine daily filter samples collected by a national network: 1. Determination of the impact of biomass burning in the upper midwest. *Journal of Geophysical Research*, *116*(D8), D08302. https://doi.org/10.1029/2010JD014166

Sullivan, A. P., Guo, H., Schroder, J. C., Campuzano-Jost, P., Jimenez, J. L., Campos, T., et al. (2019). Biomass burning markers and residential burning in the WINTER aircraft campaign. *Journal of Geophysical Research: Atmospheres*, *124*(3), 1846–1861. https://doi.org/10.1029/2017JD028153

Sullivan, A. P., May, A. A., Lee, T., McMeeking, G. R., Kreidenweis, S. M., Akagi, S. K., et al. (2014). Airborne characterization of smoke marker ratios from prescribed burning. *Atmospheric Chemistry and Physics*, *14*(19), 10535–10545. https://doi.org/10.5194/acp-14-10535-2014

Sullivan, A. P., Pokhrel, R. P., Shen, Y., Murphy, S. M., Toohey, D. W., Campos, T., et al. (2022). Examination of brown carbon absorption from wildfires in the western US during the WE-CAN study. *Atmospheric Chemistry and Physics*, *22*(20), 13389–13406. https://doi.org/10.5194/acp-22-13389-2022

Tao, Y., Moravek, A., Furlani, T. C., Power, C. E., VandenBoer, T. C., Chang, R. Y.-W., et al. (2022). Acidity of size-resolved sea-salt aerosol in a coastal urban area: Comparison of existing and new approaches. *ACS Earth and Space Chemistry*, *6*(5), 1239–1249. https://doi.org/10.1021/acsearthspacechem.1c00367

Tao, Y., & Murphy, J. G. (2019). The sensitivity of $PM_{2.5}$ acidity to meteorological parameters and chemical composition changes: 10-year records from six Canadian monitoring sites. *Atmospheric Chemistry and Physics*, *19*(14), 9309–9320. https://doi.org/10.5194/acp-19-9309-2019

Tao, Y., & Murphy, J. G. (2021). Simple framework to quantify the contributions from different factors influencing aerosol pH based on NH_x phase-partitioning equilibrium. *Environmental Science & Technology*, *55*(15), 10310–10319. https://doi.org/10.1021/acs.est.1c03103

Tian, D., & Niu, S. (2015). A global analysis of soil acidification caused by nitrogen addition. *Environmental Research Letters*, *10*(2), 024019. https://doi.org/10.1088/1748-9326/10/2/024019

Van Damme, M., Clarisse, L., Whitburn, S., Hadji-Lazaro, J., Hurtmans, D., Clerbaux, C., & Coheur, P.-F. (2018). Industrial and agricultural ammonia point sources exposed. *Nature*, *564*(7734), 99–103. https://doi.org/10.1038/s41586-018-0747-1

van Vuuren, D. P., Edmonds, J., Kainuma, M., Riahi, K., Thomson, A., Hibbard, K., et al. (2011). The representative concentration pathways: An overview. *Climatic Change*, *109*(1), 5–31. https://doi.org/10.1007/s10584-011-0148-z

Wang, R., Guo, X., Pan, D., Kelly, J. T., Bash, J. O., Sun, K., et al. (2020). Monthly patterns of ammonia over the contiguous United States at 2-km resolution. *Geophysical Research Letters*, *48*(5), e2020GL090579. https://doi.org/10.1029/2020GL090579

Wexler, A. S., & Seinfeld, J. H. (1991). Second-generation inorganic aerosol model. *Atmospheric Environment, Part A: General Topics*, *25*(12), 2731–2748. https://doi.org/10.1016/0960-1686(91)90203-J

Wyer, K. E., Kelleghan, D. B., Blanes-Vidal, V., Schauberger, G., & Curran, T. P. (2022). Ammonia emissions from agriculture and their contribution to fine particulate matter: A review of implications for human health. *Journal of Environmental Management*, *323*, 116285. https://doi.org/10.1016/j.jenvman.2022.116285

Yu, X.-Y., Lee, T., Ayres, B., Kreidenweis, S. M., Collett, J. L., & Malm, W. (2005). Particulate nitrate measurement using nylon filters. *Journal of the Air & Waste Management Association*, *55*(8), 1100–1110. https://doi.org/10.1080/10473289.2005.10464721

Zahniser, M. S., Nelson, D. D., McManus, B., Kebabian, P. L., Lloyd, D., Fowler, D., et al. (1995). Measurement of trace gas fluxes using tunable diode laser spectroscopy. *Philosophical Transactions of the Royal Society of London,Series A: Physical and Engineering Sciences*, *351*(1696), 371–382. https://doi.org/10.1098/rsta.1995.0040

Zhan, X., Bo, Y., Zhou, F., Liu, X., Paerl, H. W., Shen, J., et al. (2017). Evidence for the importance of atmospheric nitrogen deposition to eutrophic lake Dianchi, China. *Environmental Science & Technology*, *51*(12), 6699–6708. https://doi.org/10.1021/acs.est.6b06135